JOURNAL REVIEW

Monoliths as Multiphase Reactors: A Review

Shaibal Roy, Tobias Bauer, and Muthanna Al-Dahhan
Chemical Reaction Engineering Laboratory, Washington University, St. Louis, MO 63130

Peter Lehner and Thomas Turek
Bayer Technology Services, Bayer AG, D-51368, Leverkusen, Germany

DOI 10.1002/aic.10268
Published online in Wiley InterScience (www.interscience.wiley.com).

Monolith reactors are being studied as a replacement for conventional multiphase reactors such as trickle-bed reactors, slurry reactors, and slurry bubble column reactors for gas–liquid–solid reactions. Reactors with monolith catalyst packing have been found to be hydrodynamically superior to existing industrial reactors. This review covers multiphase reactions carried out in monolith reactors by various researchers. It first defines the monolith reactor and looks into the geometrical aspects of monolith. The section dealing with hydrodynamics reviews pressure drop, phase holdup, flow distribution, and dispersion characteristics. This study also considers the tools used to characterize the hydrodynamic parameters and their typical values. Although the available literature is scarce, monoliths are considered to have superior mass transfer characteristics. This review lists the mass transfer correlations for each category (gas–liquid, gas–solid, liquid–solid). The last section discusses the reaction aspects of monolith reactors. The ultimate goal is to implement such reactors for multiphase reactions. This section also compares the performance of monolith reactors with conventional multiphase reactors and lists the various reactor models reported to predict the overall performance of monolith reactors. © 2004 American Institute of Chemical Engineers *AIChE J,* 50: 2918–2938, 2004

Keywords: monolith, structured packing, hydrodynamics, Review

Introduction

Among the various chemical reactions occurring in broad range of industrial application areas, catalytic gas–liquid–solid reactions are widespread. These reactions occur extensively in chemical, petroleum, petrochemical, biochemical, material, and environmental industrial processes for a wide variety of products (such as hydrogenation, oxidation, and alkylation). Two notable examples are the catalytic hydrogenation of petroleum fractions to remove sulfur impurities and the catalytic oxidation of liquid hydrocarbons with air or oxygen (Levenspiel, 1996).

Correspondence concerning this article should be addressed to M. Al-Dahhan at muthanna@che.wustl.edu.

Different types of reactors have been used for three-phase gas–liquid–solid reaction applications. The major ones are the stirred tank slurry reactor, the slurry bubble column reactor, and the packed-bed reactor. The choice is governed by the reaction chemistry, the ease of use and manufacture of reactor types, and the enhancement of mass transfer for mass transfer limited reactions. Each reactor type has its own advantages and drawbacks. Slurry catalysts are very small (micrometer scale, 5–50 μm), whereas packed-bed particles are larger (millimeter scale, 1–3 mm). In general it can be stated that larger particles are kinetically less efficient because of intraparticle diffusion limitation. The solid–liquid slurry and the slurry bubble column reactors offer very simple reactor geometry, high heat removal, excellent mass transfer characteristics, and a high effectiveness factor because of the very small particle size. The solid catalyst is suspended in the liquid medium through which

gas is dispersed. The major disadvantages of these reactors are the separation of product and catalyst, and catalyst attrition. The filtration of fine particles, needed to separate the catalyst from liquid product, often makes this an inconvenient reactor type. A packed-bed reactor, such as the trickle-bed reactor (TBR), is much more convenient, although larger particles must be used to guarantee moderate pressure drop. In these reactors, gas and liquid flow cocurrently downward over the catalyst. Liquid flowing in a bed tends to form channels and bypasses—maldistribution of reactants is unavoidable. On the catalyst surface, where the liquid is either depleted or imperfectly covers the catalyst surface, dry areas are encountered: these substantially reduce the liquid–solid contacting efficiency of the trickle-bed reactor. Moreover, local hot spots may develop and cause runaways. Adding to the problem are the low gas–liquid velocities required to avoid excessive pressure drop. This requirement results in high operational costs and low productivity. Another major drawback of conventional reactors for multiphase reactions is the difficulty of scale-up to industrial size units (Kapteijn et al., 2001).

To overcome the above-mentioned difficulties, research has led to the use of structured packing instead of a random packed bed.

There are different types of structured packing: packing made of regular ceramic or metal support is called "monolith," whereas other types include "sandwich packing" and "open cross flow structures." The characteristic features of these types of packing are uniform flow distribution, low pressure drop, and enhanced mass transfer. The main advantage, and the explanation of its noticeable performance enhancement, lies in the manner how gas, liquid, and catalyst contact. As a result of the application of regular structure, the scale-up to industrial relevant size is considerably easier.

Through the application of these new structures, traditional unit operations and reactors can be replaced by new, highly productive and energy-efficient reactors. The new reactors will provide more process security, less by-product, and reduced dimensions for the same productivity. Stankiewicz and Moulijin (2000) described these novel developments, which have led to dramatic improvements in equipment and methods, such as process intensification.

This article will consider only the use of monolithic catalyst carrier for gas–liquid–solid reaction systems.

Monoliths have been successfully used for the abatement of NO_x and CO emissions from automobile engines and in mass transfer operations such as distillation and absorptions (Cybulski et al., 1998; Ellenberger et al., 1999).

However, their potential for use in multiphase reactions has not yet been fully realized. For slurry, trickle-bed, and monolith reactors, a number of experimental and theoretical comparisons have been made between typical parameters of catalytic gas–liquid reactions (see, for example, Mazzaroni et al., 1987; Nijhuis et al., 2001; Stankiewicz et al., 2001). These studies clearly show the superior behavior of the monolithic reactor over traditional three-phase reactors with respect to productivity and selectivity. Currently, Akzo Nobel produces hydrogen peroxide on a large scale using a monolith catalyst for the hydrogenation of anthraquinone to the corresponding hydroquinones (Albers et al., 2001). However, for successful application uniform gas–liquid distribution is inevitable because redistribution of gas–liquid flow over the reactor length is not possible.

This work reviews recent advances made in the use of monoliths as multiphase flow reactors. The review starts by defining the monolith structure, and then explores various hydrodynamic parameters, such as flow regime, liquid holdup, pressure drop, and dispersion. This is followed by a section dealing with mass transfer characteristics. These parameters are needed to predict the overall performance, design, and scale-up of monolith reactor systems. The overall performance is most frequently based on the intrinsic rate of model reactions on monolith catalyst; thus, various kinetic measurements performed on such catalyst supports at an intrinsic rate level are reported as well. Finally, the section on reactor performance reviews the performance of monolith reactor systems, combining the hydrodynamic and kinetic parameters.

We attempt to summarize what is known about hydrodynamics, transport phenomena, and kinetics in monolith reactors for three-phase applications. It is hoped that this will stimulate additional research activities, which is need to further advance our understanding of this reactor type.

Monolith Structure

The pace of research on monoliths as multiphase reactions has picked up in the last decade. Although most of the studies are presently confined to the laboratory and pilot scale, work on the hydrogenation of alkylanthraquinones in hydrogen peroxide production has reached full-scale operation (Albers et al., 2001; Schöön, 1989). This section describes the characteristic features of the monolith structure for the use as multiphase reactor packing at the laboratory scale.

Monolith structures are essentially a single structure with many thin, vertical, parallel channels, separated from each other by walls. The channels are usually rectangular, but triangles, hexagons, or more complex geometries also exist. To increase the surface area, internal fins can also be provided. Furthermore, the fins have a stabilizing effect on the gas–liquid flow and allow operation in countercurrent mode without flooding (Lebens et al., 1997, 1999a,b,c). To enhance turbulence inside monolith channels, patented monolith structures have also been developed in which either corrugation has been provided or channels have been interconnected for radial transport (Cybulski et al., 1998). Obviously, hydrodynamics of such specialty monoliths will be different from that of the straight-channel monoliths. Such details are currently unavailable in the open literature.

The number of channels per cross section, the "cell density," typically ranges between 100 and 1200 channels per square inch (cpsi). The void fraction varies between 0.5 and 0.9 and is frequently expressed as the open frontal area (*OFA*). Typical values for the wall thickness range between 0.006 and 0.05 cm. A monolith structure is characterized by the wall thickness and cell density, which are independent of each other. Various geometric parameters related to a monolith having a square cross section are listed below and correspond to Figure 1.

Cell Density

$$n = \frac{1}{L^2} \tag{1}$$

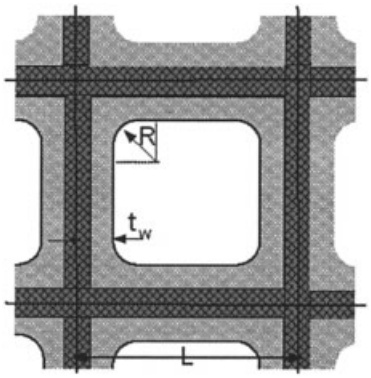

Figure 1. Cross-section of a single cell (not to scale).

Open Frontal Area

$$OFA = n(L - t_w)^2 = \frac{(L - t_w)^2}{L^2} \tag{2}$$

Geometric Surface Area

$$GSA = 4n(L - t_w) = 4\,\frac{(L - t_w)}{L^2} \tag{3}$$

Hydraulic Diameter

$$d_h = 4\left(\frac{OFA}{GFA}\right) = \frac{(L - t_w)}{4} \tag{4}$$

The parameters in Eqs. 1–3 are defined as: t, wall thickness; L, length from one channel wall center to the other; R, fillet radius.

Monoliths are industrially produced by extrusion of a paste containing catalyst particles or by extrusion of a support on which the catalyst can be coated (washcoating). A general overview about characteristics, fabrication, and typical applications can be found in Williams (2001), Garcia-Bordeje et al. (2002), and Gulati (1998). A previous work by Lachman and Williams (1992) also gives a good introduction to monolith production, raw materials, and its application in catalytic two-phase processes.

Inside the monolith, the channels are separated by the channel walls, and therefore no radial mixing occurs. This case is similar to an ideal plug-flow reactor, and therefore the reactor yield will be high.

The operating mode and flow distribution have strong effects on the performance of these reactors. The reactor can be operated in batch and in continuous modes. In the batch mode, liquid is continuously circulated through the monolith unit until the desired conversion is met. In the continuous mode, the liquid flows only once through the monolith core. There are three different flow arrangements possible: cocurrent downflow, cocurrent upflow, and countercurrent flow. Different types of distributors can be used to achieve the desired uniform flow distribution over the monolith cross section. Literature cites the use of spray nozzles, shower heads, and ejectors for downflow (Broekhuis et al., 2001; Hatziantoniou et al., 1984; Satterfield et al., 1977), and hole plates, glass frits, and static mixers for upflow mode (Thulasidas et al., 1995b); still other variations exist.

Several configurations of the monolith reactor setup are found in the literature. In the "monolith froth reactor," reactant mixture in the form of a froth is passed upward in the reactor (Crynes et al., 1995; Thulasidas et al., 1995b). In the "in-line monolith reactor," the monolith pieces are incorporated in the pipes carrying reactants (Stankiewicz et al., 2001). In the "mononolith loop reactor" (Heiszwolf et al., 2001a), and in the "ejector-driven monolith loop reactor" (Broekhuis et al., 2001), the gaseous reactant is sucked into the reactor by the liquid flow, making a closed loop of gas flow. The basic element in these reactors is the monolithic support; however, they vary with respect to cell density and void fraction. They also vary in hydrodynamics, such as in the direction of flow and recirculation of the liquid and the gas phases.

In general, in multiphase reactors it is preferable to have a high mass transfer rate to the catalyst surface. This rate can be achieved by a high surface-to-volume ratio and a short diffusion length of gas through the liquid. The monolith structure provides a very high ratio, especially for monoliths with high cell density. For example, a monolith with a cell density of 600 cpsi and an open frontal area of 82% has a surface-to-volume ratio of 3476 m^2/m^3 (data provided by Corning, Inc.). A short diffusion length can be obtained by operating the monolith in two-phase slug flow (Taylor flow) or in the annular flow regime. Taylor flow is characterized by a train of liquid slugs and gas bubbles moving consecutively upward or downward through the channel. The gas bubble length is several times the channel diameter, and the gas bubble diameter is almost equal to the channel diameter, so just a thin liquid film separates the gas from the wall. Typically, the liquid film thickness is in the range of 30 to 70 μm (Irandoust et al., 1989a; experiments in a circular glass capillary). The annular flow regime is characterized by the flow of liquid along the channel wall as a thin film and gas flow in the core of the channel. This regime can be achieved for low liquid and high gas flow rates.

In summary, the primary advantages of the monolith packing are low pressure drop in the channels and high mass transfer rates attributed to small diffusion paths. Therefore, carrying out equilibrium-limited reactions, such as hydrogenation and partial oxidation in monoliths, is a promising proposition. Moreover, many hydrogenation reactions of industrial relevance are consecutive reactions, and for such reactions, monoliths have been shown to perform better with respect to productivity and selectivity (Nijhuis et al., 2001).

Hydrodynamics

One of the most important criteria for selection of a multiphase reactor is choosing appropriate hydrodynamics (Krishna et al., 1994). Apart from high conversion, factors such as low pressure drop, high operating velocities without flooding and instabilities, the extent of axial mixing, and the proper distribution of reactant for effective utilization of catalyst are part of the wish list for reactor design. A basic understanding of hydrodynamics of monolith reactors is essential to their design, scale-up, scale-down, and performance.

Researchers in this field range from experiments to develop models for predicting the results *a priori*. Experimental studies

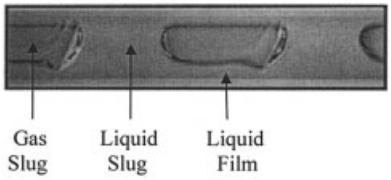

Figure 2. A monolith channel operated in slug-flow regime (from Coleman et al., 1999).

have primarily been conducted in single circular capillary tubes, for ease of visualization, but have also been conducted in laboratory-scale monoliths (1–5 cm diameter). Researchers have developed both simple semiempirical correlations as well as detailed numerical simulations, taking into account all the possible physics.

The hydrodynamic parameters such as flow regime, two-phase flow pressure drop, and liquid-holdup mainly depend on superficial liquid and gas velocities, physical properties of the fluids, as well as on the type of structured packing used, such as random packing, monolith, static mixer, or any other structure. Furthermore, it also depends on the mode of operation: whether it is operated cocurrently or countercurrently, upflow or downflow, and so forth.

This section reviews the following: the flow regime normally encountered in small-diameter capillary tubes as well as in monoliths for a range of gas and liquid velocities; studies on pressure drop in monoliths and delineate the relevant correlations; and the gas–liquid holdup (most often, though, the pressure drop studies are related to holdup calculations and axial dispersion). A major concern of researchers dealing with multiphase reactors is the gas–liquid distribution inside the reactor and the means to achieve uniform distribution. There is a general disagreement among researchers regarding the degree of axial and radial dispersion in monoliths. Some of the studies reviewed in this section have found the dispersion to be significant.

Flow regime

A number of flow regimes have been identified in capillary channels. These regimes are dispersed bubbly flow, slug flow (Taylor flow) (see Figure 2), churn flow, and annular flow. Primarily, these studies have been carried out by researchers studying heat exchangers or in the field of nuclear engineering (Coleman et al., 1999; Mishima et al., 1996; Triplett et al., 1999a,b; Zhao et al., 2001). The common aim of these researchers is to establish maps to visualize the flow pattern inside the capillaries and to define the transition areas and flow pattern maps using gas and liquid superficial velocities as coordinates.

In a more recent study, Mishima et al. (1996) performed experiments in capillary tubes. Figure 3 shows an experimentally developed flow regime map for a glass capillary of 2.05 mm diameter, in which the model correlations developed for large diameter tubes have been superimposed. Similar flow maps from 1.05-, 3.12-, and 4.08-mm tubes are also available (Mishima et al., 1996).

In the world of monoliths, similar flow regimes exist but they are difficult to visualize. Because of the opaque nature of the monolith material and the small hydraulic diameter of the channels, it is virtually impossible to determine the flow characteristics and flow regime changes inside the monoliths. Therefore, new noninvasive measurement techniques, such as magnetic resonance imaging (MRI), can aid in depiction of flow regimes inside monoliths. Two recent reports on the use of MRI to determine slug flow were published by Mantle et al. (2002) and Gladden et al. (2003). The extension of the application to other flow regimes is desirable. Table 1 summarizes the work performed in single capillary tubes and monoliths.

The choice of the particular regime for industrial applications depends on the nature of reaction and the process conditions. Flow regimes are mainly influenced by the gas and liquid properties, superficial velocities, and the diameter of the capillary and monolith channel.

The overall gas–liquid holdup, pressure drop, and distribution inside the reactor depend on the flow regime in which the reactor is working.

Most of the authors have described the flow regimes as consisting of bubbly flow at low gas and high liquid velocities. They have found slug flow, churn flow, and annular flow at high gas and low liquid flows, as shown in Table 1.

Although the above regimes were observed in cocurrent upflow, any difference in downflow regimes caused by the difference in flow direction is small because of the relatively negligible influence of gravitational force in capillary tubes (Cybulski et al., 1998).

In the real world of monoliths, it remains to be seen how capillary analysis can be extended to monolith beds, considering the fact that the monolith channels are mostly noncircular in cross section and the surface roughness properties could be significantly different from those of glass tubes. It is questionable whether the exiting theories obtained from experiments in capillary tubes can be extended to monoliths. Further investigations into the effects of capillary forces, caused by sharp corners of noncircular channels on the two-phase flow pattern, are inevitable. The authors believe that only noninvasive measurement techniques, such as MRI in conjunction with the consideration of the gas/liquid distribution device, can provide

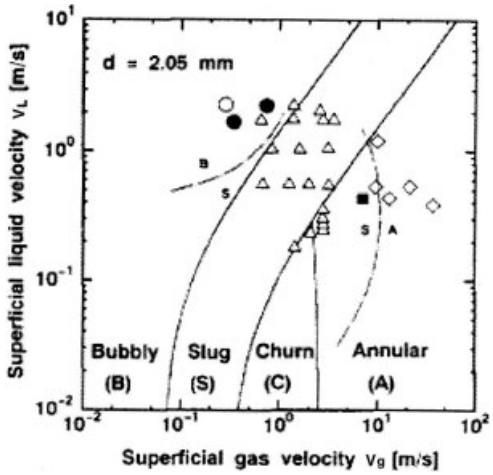

Figure 3. Flow regime map in a single capillary (d = 2.05 mm).

The open symbols indicate clearly identified flow regimes and the solid symbols fall in the gray areas (from Mishima et al., 1996).

Table 1. Summary of Flow Regime Studies

Reference	Structure and Flow	Flow Range	Reactor Dimensions	Flow Regimes Studied
Scatterfield et al., 1977	Monolith with three different distributors	Air–water	L_R = 122 cm	Annular flow, slug flow
		Air–cyclohexane	D_R = 2.54 cm	
		u_L = 0.33 to 6.58 cm/s	n = 200 or 360 cpsi	
	Cocurrent downward	u_G = 0–150 cm/s	Block length = 7.6 or 15.2 cm	
Irandoust et al., 1989a	Capillary glass tube	Liquid loading = 0.04 to 0.43 m^3/m^2 s	L_R = 200 mm	Slug flow
	Cocurrent downward	u_{tot} = 0.27 to 0.53 m/s	d_c = 1.5 mm	
Mishima et al., 1996	Capillary tube	Air–water	d_c = 1.05–4.08 mm	Bubbly flow, slug flow, churn flow, annular flow
		$u_L \sim$ 0.01–0.91 m/s		
	Cocurrent upflow	$u_G \sim$ 0.09–80 m/s (depending on d_c)		
Reineck et al., 1996	Monolith	u_L = 0–0.2 m/s	L_R = 2 m	Bubbly flow, plug flow, aerated slug flow, annular flow
		u_G = 0–8 m/s	D_R = 118 mm	
	Cocurrent downward		n = 300 and 400 cpsi	
Lebens et al., 1997	Monoliths with internal fins and beveled ends	n-Decane–air	L_R = 0.5 m	Annular flow
		u_L = 0.009–0.05 m/s	d_c = 4.5 mm	
	Countercurrent	u_G = 0–5 m/s		
Mewes et al., 1999	Monolith, TBR	u_L = 0.01–0.14 m/s (without air)	L_R = 30 mm	Slug flow unaerated, aerated
	Cocurrent downward	u_L = 0.26–0.39 m/s	D_R = 120 mm	
		u_G = 0–5 m/s	d_c = 2 mm	
Coleman et al., 1999	Glass capillary	u_L = 0.01–10 m/s	d_h = 1.3 to 5.5	Bubbly, dispersed and elongated bubbly flow, slug flow, wavy, annular wavy and annular flow
	Cocurrent vertical flow	u_G = 0.1–100 m/s		
Triplett et al., 1999a,b	Glass capillary	u_L = 0.02–8 m/s	d_c = 1.1 and 1.45 mm	Bubbly flow, churn flow, slug flow, annular flow
	Cocurrent vertical flow	u_G = 0.02–80 m/s		
Zhao et al., 2001	Triangular glass capillary	u_L = 0.1–10 m/s	d_h = 0.866, 1.443, and 2.886 mm	Dispersed bubbly flow, slug flow, churn flow, annular flow
	Cocurrent upflow	u_G = 0.1–100 m/s		

proper flow maps and transition criteria for monoliths. Unfortunately, such a technique is costly, limited to reactor scale, and only a few research groups work on this topic. Furthermore, pressure drop measurements could give important information about the flow regime and flow regime transitions inside the monolith bed.

Moreover, the turbulent regime should be more thoroughly investigated because it could significantly enhance the productivity at a pressure drop comparable to that of packed-bed reactors. The factors influencing the instabilities in flow and transition from one regime to another need to be thoroughly investigated.

Pressure drop

Operations of multiphase processes, especially packed-bed reactors, are always associated with pressure losses because of the inner design of the reactors. Pressure drop represents the energy dissipated caused by fluid flow through the reactor bed. It is important in determining the energy losses, the sizing of the compression equipment, liquid holdup, gas–liquid interfacial area, and mass transfer coefficient (Al-Dahhan et al., 1994). High pressure drop through the system not only requires high energy input to the system, it also prohibits the unit from being operated at high gas and liquid velocities, and thus the throughput is limited. The use of novel structured catalystic packing like monoliths addresses these concerns and reduces investment and operation costs.

Starting from Ergun (1954), the estimation of pressure drop along packed beds has been well documented over the years. Besides a number of empirical correlations (Pinna et al., 2001) phenomenological models have also been developed (Al-Dahhan et al., 1997).

As mentioned earlier, one of the major advantages of structured packing is low pressure drop along the bed, which enables the unit to run at higher capacity without encountering hydrodynamic instability. Table 2 lists the pressure drop cor-

Table 2. Pressure Drop Equations and Correlations for Capillaries and Monoliths

Author	Pressure Drop Equation and Correlation	
Standard pressure drop expression	Frictional pressure drop per unit length of single phase:	
	$\left(\frac{\Delta P}{L}\right)_{f,i} = 2f\frac{\rho_i u_i^2}{d_h}$	(5)
	Friction factor (Darcy, Fanning):	
	$f = \frac{f_D}{8} = \frac{f_F}{2}$	(6)
	For laminar flow, Re $<$ 2100 (Hagen–Poiseulle law):	
	$f_D = \frac{64}{\mathrm{Re}} \qquad f_F = \frac{16}{\mathrm{Re}}$	(7)
	$\left(\frac{\Delta P}{\Delta L}\right)_i = \frac{32\mu\rho_i}{d_h^2} \qquad (i = G, L)$	(8)
Satterfield et al. (1977)	$\Delta P_m = \Delta P_f + \Delta P_{or} - g\rho_L L\varepsilon_L$	(9)
	$\Delta p_{orif} = \frac{N(V_{orif}^2 - V_{iot}^2)}{2}[\varepsilon_L\rho_L + (1-\varepsilon_L)\rho_G]$	(10)
Grolman et al. (1996)	$\Delta P = \Delta P_{TP,f} + \Delta P_G$	(11)
	$\Delta P_{TP,f} = \varepsilon_L \frac{64}{\mathrm{Re}_{TP}}\frac{L}{d_c}\frac{1}{2}\rho_L(u_L + u_G)^2$	(12)
	$\Delta P_G = Cu_G \qquad \text{with} \qquad C = 45{,}000 \text{ Pa s}^{-1} \text{ m}$	(13)
Mewes et al. (1999)	$\frac{\Delta P}{\Delta L} = -\varepsilon_L\rho_L g + 32\mu_L\frac{u_L}{d_C^2} + 32\mu_G\frac{u_G}{d_C^2} + \frac{\rho_L}{2}(u_L + u_G)^2\frac{\varepsilon_{gG}}{L_b}$	(14)
	$\frac{\varepsilon_{gG}}{L_b} = \frac{(1-\varepsilon_G)0.15}{L_{b0}(1-0.15)} \qquad \varepsilon_G \geq 30\%$	(15)
	$\frac{\varepsilon_{gG}}{L_b} = \frac{\varepsilon_G}{L_{b0}} \qquad \varepsilon_G \leq 30\%$	(16)
Heiszwolf et al. (2001a)	Entry-region friction model:	
	$f_{TP}\mathrm{Re}_L = (f\,\mathrm{Re})_L\varepsilon_L\left[1 + 0.065\left(\frac{L_b}{d_c\mathrm{Re}_L}\right)^{-0.66}\right]$	(17)
Heiszwolf et al. (2001a)	$\left(\frac{\Delta P}{\Delta L}\right) = -f_{TP}\frac{1}{2}\rho_L u_{TP}^2\frac{4}{d} + \varepsilon_L\rho_L g$	(18)
	$f_{TP} = \frac{F}{\mathrm{Re}_{TP}} \qquad \mathrm{Re}_{TP} = \frac{\rho_L u_{TP} d_h}{\mu_L}$	
	$F = 18$ (200 cpsi, OFA = 0.74)	
	$F = 22$ (400 cpsi, OFA = 0.75)	
	$f = 28$ (600 cpsi, OFA = 0.79)	
	Pseudo-homogeneous model:	
	$f_{TP}\mathrm{Re}_L = \text{const}$	
Lebens et al. (1999)	$\nabla(\mu_i\nabla U_{iZ}) = \frac{dp}{dz} + g\rho_i$	(19)
	with $i = G, L$	

relations reported by researchers working in the field of monolith.

The pressure drop through the monolith is primarily caused by factors such as (1) the wall friction, (2) the acceleration of gas phase, (3) the orifice effect at the entry region and between the monolith stacks, and (4) pressure drop caused by the gas–liquid distributor. Mewes et al. (1999) also considered the pressure drop attributed to aeration of liquid slugs, which depends on the number of bubbles formed in the liquid slugs (Table 2). If we assume the phases moving along the monolith channel to be incompressible, the pressure drop caused by the acceleration can be neglected.

In all the correlations listed in Table 2, the pressure drop attributed to wall friction has been modeled in line with Hage-

n–Poiseulle law. For specific monoliths, the friction factors have been calculated experimentally as well as theoretically (assuming laminar flow) with good agreement. In general, the pressure drop attributed to the gas phase was found to be very small.

Considerably less attention has been given to the last two factors (orifice effects and distributor pressure drop). Satterfield and Özel (1977) used the Bernoulli relationship to model pressure drop resulting from orifice effects. However, the authors found this contribution to be small compared to that of friction losses.

Heiszwolf et al. (2001a) explained the phenomenon of bubble formation in the liquid slugs and its effect on the pressure drop. When gas bubbles in the channel are entirely contained within the liquid and do not interact with the wall, the pressure drop is high because of higher friction of liquid. When enough gas is introduced, two counteracting effects take place. The friction factor decreases because of gas friction with the wall (which is less than liquid friction), but it also, to some extent, reduces the laminar nature of the liquid slugs and thus increases the friction factor. The authors proposed a two-phase friction factor f_{TP} to model the pressure drop.

Clearly, there is a greater need to investigate the entrance and exit effects, particularly the role of gas bubbles of varying size on the pressure drop. Researchers have used various types of distributors in conducting experiments related to monoliths. Most often, however, only the pressure drop across the monolith has been reported, which could lead to undersizing of pumps and compressors while designing a monolith unit.

Finally, it is important to investigate pressure drop in flow regimes other than slug flow. In some of the recent investigation related to monolith, researchers are investigating the application of monoliths in annular flow (Roy et al., 2002).

Holdup

Gas–liquid holdup is an important hydrodynamic parameter for reactor design, scale-up, and performance modeling. Considerable research has been performed on packed-bed and trickle-bed reactors to determine phase holdup, and reviews are available in the literature (see, for example, Al-Dahhan et al., 1999). Several methods have been used to measure the holdup, including gravimetric method (Nemec et al., 2001) for overall holdup and the tomographic method for cross-sectional holdup (Boyer et al., 2002; Chen et al., 2001). Determination of holdup and holdup distribution is as important in structured beds as it is in packed beds. The flow regimes significantly affect the holdup. In structures such as sandwich beds and trickle beds, the regimes are considerably different from those in monolith because of the difference in flow paths. In monoliths, the holdup is characterized by the formation of liquid slugs in the channels in a regular fashion, whereas the liquid holdup in trickle beds and other structured bed reactors arises from rivulets between the particles and structures.

In monoliths operating in the Taylor flow (slug flow) regime, the liquid holdup is simply the ratio of average liquid slug length to the total length of the liquid and gas slug combined, neglecting the contribution of liquid film surrounding the gas bubble. This is true when the slugs do not coalesce, which is the case reported by most investigators (Cybulski et al., 1998; Grolman et al., 1996). Mewes et al. (1999) quoted previous researchers in this field to predict that the ratio between the average velocity of the liquid slugs and the average velocity of bubbles differs only slightly from one. Thus, the average volume fraction of gas equals approximately the ratio of the flow rate of gas to total flow rate, with a difference of about 15%. It is therefore obvious that the proper measurement of the length of the liquid and gas slug would give a fairly reliable measure of the holdup.

Ishii (1977) investigated two-phase flow in round tubes and developed the drift-flux (D-F) model to describe the relative motion between phases in flow regimes. According to the D-F model, the relationship between the gas velocity and the mixture's volumetric flux is expressed in Eq. 22 (Table 3). Later, Mishima et al. (1996) provided a new distribution parameter for two-phase flow in small diameter vertical tubes. This parameter was obtained from experiments in tubes with inner diameters ranging from 1 to 4 mm, operated in bubbly flow and slug-flow regimes.

Various techniques have been used to measure the lengths of gas and liquid slugs. Hatziantoniou et al. (1984) and Irandoust et al. (1988a) used two different techniques in a cocurrent downflow mode. First, they measured the displacement of the pump piston, which gives the liquid slug length, and measured the frequency of the stroke for the gas bubble length. Second, they used of a conductivity cell, whose response is shown in Figure 4. Two probes were installed at the exit of a monolith channel. One was placed at the center of the channel, the other one at the channel wall.

The results obtained by the two methods were within 9.5% of each other. It was also observed that the lengths of the gas and liquid slugs could be independently varied by changing the corresponding flow rates.

In subsequent works, Irandoust et al. (1989, 1992) used a photocell to visualize the flow regime and to measure the plug lengths in a glass capillary of diameter 2.2 mm. The lengths of the gas slugs varied from 3.4 to 29.1 mm, and those of the liquid varied from 2.9 to 67 mm, for a total average linear velocity of 0.092 to 0.56 m/s.

Grolman et al. (1996) performed direct integral holdup measurements. The liquid holdup was obtained by continuously weighing the column. Furthermore, a model was presented that takes into account the liquid slug and the liquid film between the gas bubble and the wall. The experimental values are in good agreement with the model prediction for liquid holdup values higher than 65%. The authors assume that the discrepancies at lower liquid holdup are caused by liquid maldistribution.

Few researchers have considered holdup measurements in flow regimes other than Taylor flow. The focus of their investigations has been the annular or film flow regime in countercurrent and cocurrent downflow mode. The annular flow regime is akin to film flow: the liquid trickles down the corner of the channels and the gas occupies the core.

Heibel et al. (2001a) successfully used magnetic resonance imaging (MRI) to measure the holdup inside the monolith in the film-flow regime. They used a cell density of 25 cpsi and operated the monolithic reactor in downflow mode. Water velocity was varied from 0.45 to 4 cm/s, and no gas flow was used. Within the range of flow rates the liquid holdup varied between 4 and 15%. The system was also modeled by solving Navier–Stokes equations, assuming no slip between the gas

Table 3. Holdup Correlations for Capillaries and Monolith Channels

Author (Year)	Holdup Correlation	
Wallis (1969)	$\varepsilon_G = \dfrac{\phi_G}{(\phi_G + \phi_L)} = \dfrac{u_G}{(u_G + u_L)} = \beta$	(20)
Butterworth (1975)	$\dfrac{1-\varepsilon_G}{\varepsilon_G} = A\left(\dfrac{1-x}{x}\right)^p \left(\dfrac{\rho_G}{\rho_L}\right)^q \left(\dfrac{\mu_L}{\mu_G}\right)^r$	(21)
	For Lockart–Martinelli (1949) correlation:	
	$A = 1.0,\ p = 0.64,\ q = 0.36,$ and $r = 0.07$	
	For Broncy (1963) correlation:	
	$A = 1.0,\ p = 0.74,\ q = 0.65,$ and $r = 0.13$	
Ishii (1977)	$v_G = u_G/\varepsilon_G = C_0(u_G + u_L) + V_{G,u}$	(22)
	$\varepsilon_G = \dfrac{u_G}{C_0(u_G + u_L) + V_{G,u}}$	(23)
	Slug flow:	
	$C_0 = 1.2 - 0.2\sqrt{\rho_G/\rho_L}$	(24)
	$C_0 = 1.2 + 0.51e^{-0.691 d_c}$ (Mishima et al., 1996)	(25)
	$V_{G,u} = 0.35\sqrt{\Delta\rho g d_c/\rho_L}$	(26)
Grolman et al. (1996)	$\varepsilon_L = \dfrac{u_L + u_G(1 - R_0^2/R^2) - \phi_{LF}/\pi R^2}{(u_L + u_G) - \phi_{LF}/\pi R^2}$	(27)

and liquid interface, and the model's predicted holdup was in very good agreement with the MRI results except at low liquid flow rates ($U_l < 0.75$ cm/s).

In general, the gas and liquid velocities inside the monolith channels can be independently varied by changing the gas and liquid flow rates into the system. Therefore the holdup can be changed either by changing liquid or gas flow rates. Broekhuis et al. (2001) and Heiszwolf et al. (2001a) described a monolith loop reactor in which gas is recirculated within the system using an ejector driven by liquid flow. The gas recirculation velocity depends on the liquid velocity, the two being related because of the equilibrium of pressure drop in the monolith section and recirculation section. Therefore the gas holdup cannot be independently changed and depends entirely on the liquid velocity. Because the pressure drop in the two sections also depends on the total pressure of the system, by changing this pressure, the gas velocity and thus the gas holdup can be changed to some extent.

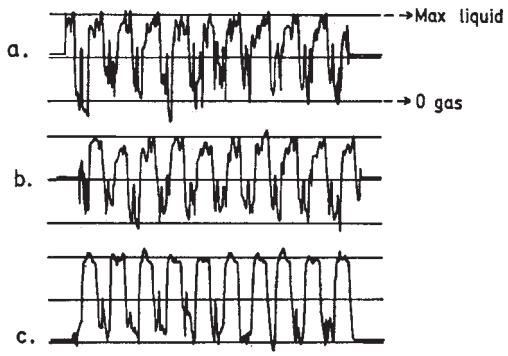

Figure 4. Conductivity cell response at three different gas/liquid flow rates.

(a) $u_L = 16.7$ cm^3/s, $u_G = 15.6$ cm^3/s; (b) $u_L = 16.7$ cm^3/s, $u_G = 27.0$ cm^3/s; (c) $u_L = 10.8$ cm^3/s, $u_G = 15.6$ cm^3/s, channel cross section 2.0 mm^2, bed porosity 59% (from Hatziantoniou et al., 1984).

Unfortunately, most of the research performed in this field does not address the concern of holdup distribution across the monolith cross section, which can prove to be an important parameter for reactor design. Recently, noninvasive techniques such as capacitance, X-ray and γ-ray tomography, and MRI have been successfully used in conventional reactors as well as in structured beds (Harter et al., 2001; Heibel et al., 2001b; Kumar et al., 1997; Mewes et al., 1999; Reinecke et al., 1998) and can be extended to study the holdup distribution in monolith packing.

Flow distribution

Uniform flow distribution in a multiphase reactor is important for enhanced productivity and selectivity. It ensures complete use of the catalyst and prevents hot spots in an exothermic reaction system. For conventional reactors such as packed beds, slurry columns, and bubble columns, distributions of the gas and liquid phases have been studied in detail (Marcandelli et al., 2000), including various techniques used to measure flow maldistribution. The same measurement techniques have been extended to a structured bed as well. The importance of gas/liquid distribution inside monoliths is much more profound because, unlike random packing or other structured packing, once the liquid enters the reactor, there is no further redistribution inside the monolith. Therefore the liquid must be distributed uniformly before it enters the monolith bed.

Several ways have been devised by various researchers for liquid distribution in monoliths operating in gas–liquid cocurrent downflow mode. A showerhead was the most widely used distribution device (Hatziantoniou et al., 1984, 1986; Irandoust, 1989; Nijhuis, 2001; Satterfield, 1977) because of its easy

Table 4. Summary of Distribution Systems Used by Different Researchers in Monolith

Author/Year	Direction of Flow	Distributor	Velocities	Remarks
Satterfield et al. (1977)	Downflow	Shower head layer of spheres monolith discs	u_L = 0.3 to 6.6 cm/s	Layer of monolith discs gave reproducible pressure drop values, indicating uniform distribution
			u_G = 0–150 cm/s	
Irandoust et al. (1989)	Downflow	Sieve plates	$u_L + u_G$ = 0.27 to 0.53 m/s	
Crynes et al. (1995)	Upflow	Glass frit	u_L = 0.4 to 3,5 cm^3/s	Distributor produces froth, which then travels up
			u_G = 15.8 to 50 cm^3/s	Overall monolith activity achieved was same as intrinsic rate, indicating uniform distribution
Reinecke et al. (1996)	Downflow		u_L = 0–0.2 m/s	Maldistribution observed using capacitance tomography. With increasing liquid velocity, distribution improved
			u_G = 0–8 m/s	
Mewes et al. (1999)	Downflow		u_L = 0.26–0.39 m/s u_G = 0–5 m/s	Same as above
Broekhuis et al. (2001)	Downflow	Liquid-driver ejector	u_L = up to 20.4 cm/s	The ejector action produces fine gas bubbles in liquid

construction and operation. Table 4 gives a summary of distribution systems used by different researchers.

Irandoust et al. (1989) evaluated the flow distribution in a monolith operated in downflow by using several perforated sieve plates, with perforations ranging from 5.7 to 27% open area and hole diameter from 0.5 to 2.75 mm. The experiment was performed in a column having a diameter of 25 cm. Water flowed through the distributor, whereas air made a side entry just before the monolith. It was observed that the liquid flow distribution was dependent on pressure drop across the perforated plate. The liquid was poorly distributed when the pressure drop across the plate fell below 100–200 mm of water and resulted in a much thicker spray of liquid over the monolith channels. According to Cybulski et al. (1998), the liquid spray drops should be much smaller than the channel diameter and should be sprayed uniformly over the monolith.

Satterfield et al. (1977) investigated three different types of liquid distributors for downflow arrangement and evaluated the results for reproducibility. First, a flat distributor head with an arrangement of 37 capillaries, varying from about 3 to 7 mm, was used. The distribution was not uniform over the cross section, which resulted in irreproducible pressure drop data. In addition, a slight rotation of the head caused significant differences in pressure drop. The second distributor was a layer of 4-mm-diameter spheres. Some of the spheres plugged the entrance of monolith channels, and flooding above the layer occurred at high liquid flow rates. This distributor also gave unusable data. The authors obtained best distribution (indicated by reproducibility of pressure drop) by using 27 randomly aligned stacks of monoliths, each 3.2 mm thick, below the showerhead.

Mewes et al. (1999) studied flow distribution in monoliths by capacitance tomography. A spatial resolution of about 5–10% of the diameter of the measurement plane is in general possible using capacitance tomography (Reinecke et al., 1999). In this study, only liquid flow distribution in a 120-mm monolithic reactor is considered. At low liquid velocities, the pressure drop across the monolith is negative (hydrostatic pressure is more than the frictional pressure drop), and this condition forced recirculation of trapped gas inside the monoliths. With increasing liquid velocity, the quality of liquid distribution increases. The effect of gas velocity on the liquid distribution was not demonstrated.

Crynes et al. (1995) developed a novel "monolith froth reactor" in which a gas–liquid froth was made to flow up under pressure. The froth was prepared by passing gas through a glass frit (145- to 175-μm pore diameter) over which liquid was flowed. The system was tested for aqueous oxidation of phenol in a γ-alumina washcoat monolith impregnated with CuO as active metal. The observed reaction rate was close to the intrinsic rate, which the authors interpreted as a sign of good phase distribution and minimal transport resistances.

Broekhuis et al. (2001) used a liquid-motive ejector as a gas–liquid distributor. They claim that this ejector is also a very good gas–liquid contactor, presaturating liquid before it enters the reactor. It produces a fine dispersion of gas bubbles in liquid, which results in excellent gas–liquid distribution over the cross section of the monolith. The ejector also acts as a gas compressor, resulting in higher superficial gas and liquid velocities compared to those produced by gravity-driven monolith reactors.

It is interesting to note that, in most of the studies mentioned above, the role of gas velocities on the liquid distribution has not been studied. In a critical observation of the published works, the researchers have mainly depended on indirect methods of qualitatively estimating the flow maldistribution, such as consistency in pressure drop measurement (Satterfield et al., 1977) or high reactor productivity (Crynes et al., 1995). This has resulted in no single parameter being used to quantitatively define a maldistribution and compare the performance of these distributor studied.

Modern-day noninvasive tools such as computed tomogra-

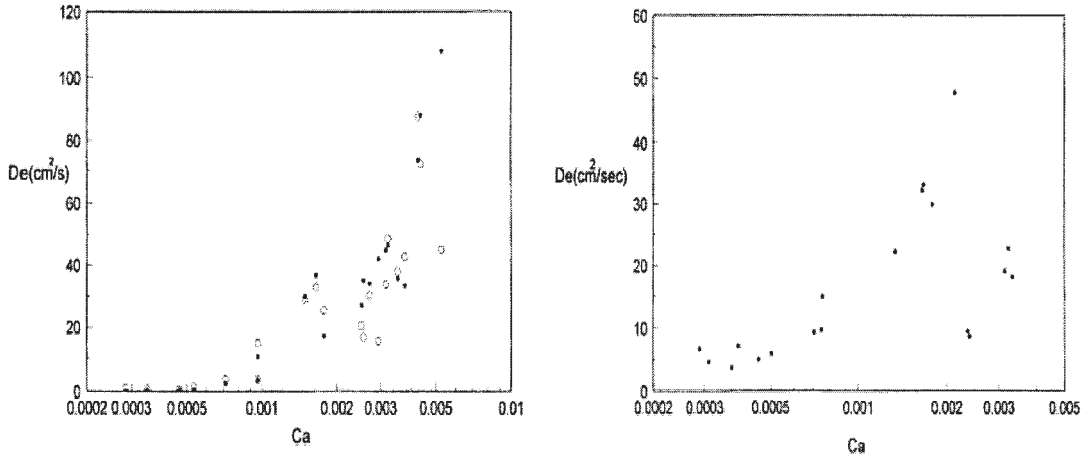

Figure 5. Axial dispersion coefficient for bubble-train flow in 2 mm.

(a) Circular capillary as a function of capillary number (Ca = $\mu v/\sigma$): ○, experimental; ■, theory. (b) Square capillaries: ■, experimental data (from Thulasidas et al., 1999).

phy, electrical and capacitance tomography, and MRI can help generate quantitative images of the gas and liquid phase on a cross section and longitudinal sections. These images will lead us to better understand the dynamics of each type of distributor.

Axial and radial dispersion

Neglecting proper characterization of the mixing phenomena can result in considerable error in the reactor performance. In packed-bed reactors, the idealized assumption of plug flow for modeling purposes is no longer pursued and considerable work has been done to develop various levels of models such as the axial dispersion model (ADM), tanks in series model, and so forth (Ramachandran et al., 1983; Sundreasan, 1986; Taylor, 1953). These models attempt to account for the flow deviation from plug flow character and to improve reactor performance.

In modeling monolith reactor performance, plug flow of the liquid slugs has most often been assumed (Cybulski et al., 1993, 1999; Edvinsson et al., 1994; Hatziantoniou et al., 1984; Irandoust et al., 1989b,c; Stankiewicz, 2001). This assumption is bolstered by the fact that in slug flow, the liquid slugs are intensely mixed (Irandoust et al., 1989b) and there is very little concentration gradient in either the radial or axial direction if no chemical reaction takes place. Moreover, the thickness of the liquid film around the gas bubbles is very small. There is thus no interaction between two successive liquid slugs, and hence axial dispersion is minimal.

In a study of residence time distribution (RTD) in monolith froth reactor in cocurrent upflow, Patrick et al. (1995) observed that interaction takes place as a result of dispersion in the thin liquid film surrounding the gas slugs. A series of tracer studies, by use of 4,6-dichlororesorcinol (DCR), was conducted in a monolith reactor assembly with a cell density of 400 cpsi. The actual liquid residence time in the monolith was calculated from overall residence time measurements, using deconvolution by Fourier transform. When fitted into the experimental RTD data obtained at a liquid flow rate of 4.7 cm^3/s and a gas flow rate of 47 cm^3/s, a tank-in-series model predicted the monolith as 1.15 perfectly mixed vessel, which indicates a high degree of backmixing inside the monolith.

Thulasidas et al. (1995b) also reported modeling and experimental work to determine the liquid-phase RTD in capillary tubes of circular and square cross section, operated in upflow mode. A corresponding mathematical model was developed, based on the mass balance of the tracer element. In their model, complete mixing within the liquid slugs and transport of tracer through the liquid film surrounding the gas bubble were assumed. The model and the experimental data were in agreement for a circular capillary. It was found that the measured mean residence time for the circular capillary was 20.0 s, whereas the time predicted by the model was 19.6 s. The result confirms the small amount of backmixing in circular capillaries. However, the model failed to predict the mean residence time for square channels as well as it did for the monolith froth reactor. The experimentally obtained mean residence time for a square capillary was 27.9 s. The authors argue that the liquid slugs are not well mixed because the liquid flows through the corners of the channels. The liquid flowing through the corners of the channels will almost completely bypass the liquid slugs. It is claimed that the model can be extended to the monolith reactor by applying a statistical analysis of the flow within the channels of the monolith.

Thulasidas et al. (1999) performed tracer studies in capillaries with circular and square cross sections with a hydraulic diameter of 2 mm and also studied a capillary bundle. The bundle consisted of 96 square capillaries with a hydraulic diameter of 2 mm. The studies were carried out in upward slug flow mode. A mass transfer model was used to predict concentration vs. time curves for liquid slugs leaving the capillaries. The results show good agreement between the model prediction and the experimental data. Axial dispersion coefficients computed from experimental values of the Peclet numbers (Pe) for bubble train flow in circular and square capillaries are shown in Figures 5a and 5b.

The theoretical model was extended for a bundle of capillaries and used to estimate residence time distributions. Normalized concentration vs. time curves for the capillary bundle are shown in Figure 6a; the computed RTD for a capillary section is shown in Figure 6b. The average residence time from the distribution shown in the latter figure is 69.41 s. The model predicts well the RTD in a single capillary but for an extension

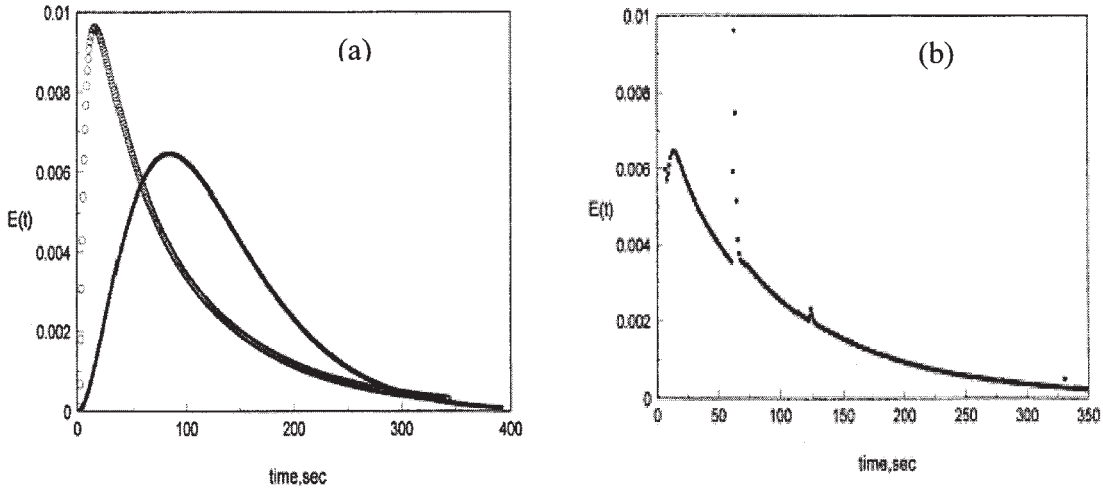

Figure 6. (a) Experimental normalized concentration distribution for liquid-only flow and bubble flow in a capillary bundle: ■, liquid flow only; ○, bubble train flow; (b) normalized concentration vs. time distribution for capillary bundle after deconvolution; ■, experimental tracer concentration vs. time distribution (from Thulasidas et al., 1999).

to capillary bundles or monoliths it needs further studies of the flow inside these arrays.

Obviously, there is an apparent disagreement among researchers about the presence of axial dispersion in monoliths. Even though cocurrent downflow operation has been assumed to be plug flow, direct experimental verification of this assumption is not available. In almost all studies, the regime of interest was slug flow (Taylor flow). However, investigating peripheral regions such as bubbly flow and churn flow will be of interest for many mass transfer limited reactions. For annular flow, the flowing film is considered laminar and treated accordingly during modeling (Roy et al., 2002).

Mass Transfer

As mentioned earlier, one of the most attractive features of monolith as compared to random packing for a multiphase reaction is its enhanced mass transfer characteristics. In the Taylor flow regime, an intense mixing takes place within the liquid slug, which significantly enhances the liquid–solid mass transfer rate. Moreover, the film separating gas plugs and channel walls is very thin, posing minimal gas–solid mass transfer resistance. Most of the correlations for liquid–solid mass transfer developed so far in random packing are based on power-law correlations relating the Sherwood number with the Reynolds number, Schmidt number, and other geometrical properties of mass transfer devices (Highfill et al., 2001). Because the mechanism of mass transfer is expected to be the same in monoliths, the same dimensionless groups may play important roles in the development of mass transfer correlations in monoliths.

The overall mass transfer rate in monolith depends primarily on four different mass transfer phenomena, as depicted in Figure 7. Because the reaction takes place on the surface and inside the pores of the washcoated wall, the gas and liquid reactants have to transfer from the bulk to the catalyst surface. The gaseous reactant diffuses from the bulk of the gas slug to the liquid bulk, and the corresponding flux depends on the gas–liquid mass transfer coefficient (k_{GL}). The transport of liquid reactant and the dissolved gas in the liquid from the bulk of the liquid to the washcoat surface depends on the liquid–solid mass transfer coefficient (k_{LS}). Gas in the gas slug also diffuses to the surface of the catalyst through the thin liquid film, which is characterized by the gas–solid mass transfer coefficient (k_{GS}). Finally, the reactants on the surface of the catalyst have to diffuse into the pores of the washcoat or the catalyst wall by standard diffusion processes. This diffusion has been dealt with extensively in standard reaction engineering text books (Fogler, 1992; Froment and Bishoff, 1990; Levenspiel, 1998) and will not be discussed in detail here. All the above information is needed to adequately model the overall performance of the reactor. In subsequent sections, we will explore each of the transport properties in detail.

Liquid–solid mass transfer

Hatziantoniou et al. (1982) studied the liquid–solid (L-S) mass transfer in capillary tubes of 2.35 and 3.094 mm diameters. The channel wall was coated with benzoic acid, and water and air were passed cocurrently downward. The outlet concentration of benzoic acid dissolved in water was measured. The L-S mass transfer coefficient was extracted from experimental results and by performing a differential mass balance on benzoic acid assuming a plug-flow behavior. Based on the experimental results, the author proposed the following correlation for the liquid–solid mass transfer coefficient

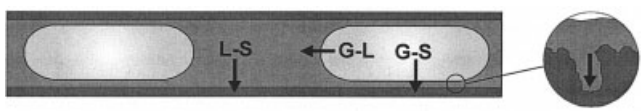

Figure 7. Different transport phenomena in Taylor flow inside a monolith.

Gas/solid (G-S), gas/liquid (G-L), liquid/solid (L-S), pore diffusion.

$$\mathrm{Sh} = 3.51\left(\frac{\mathrm{ReSc}}{\gamma}\right)^{0.44}\beta^{-0.09} \tag{28}$$

where $\gamma = L_c/d_c$ and $\beta = L_s/d_c$.

It is interesting to note that the expression contains the tube length, which makes it unsuitable for scale-up. The flow rate at which the expression was developed was significantly high so as to maintain complete recirculation within the liquid plugs, and thus the correlation cannot be used at low Reynolds numbers.

Based on a dissolution study in cylindrical capillaries, Irandoust and Andersson (1988) developed a new correlation to estimate the liquid–solid mass transfer coefficient

$$\mathrm{Sh} = 1.5 \times 10^{-7}(\mathrm{Re})^{1.648}(\mathrm{Sc})^{0.177}(\alpha)^{-2.338} \tag{29}$$

where α is the dimensionless film thickness, δ_f/d_c. The authors cited data from an unpublished work to formulate the above correlation.

Bercić et al. (1997) carried out an experiment similar to that of Hatziantoniou et al. (1982), in a glass tube of 2.5 mm diameter coated with benzoic acid. Air and water were passed through the tube in a controlled manner to form Taylor flow inside the tube. Nonlinear regression was used to fit the experimental data to a model equation to correlate the liquid–solid mass transfer coefficient with the unit cell length (*UCL*, the sum of one gas and one liquid slug length) and the cell velocity v

$$k_{LS}a = \frac{0.069\,v^{0.63}}{[(1-\varepsilon_G)UCL - 0.105UCL\varepsilon_G]^{0.44}} \tag{30}$$

Based on mass transfer experiments, Heiszwolf et al. (2001b) proposed a semiempirical liquid–solid mass transfer model

$$\mathrm{Sh} = 3.66\left[1 + 0.152\left(\frac{\Psi_s}{\mathrm{ReSc}}\right)^{-0.423}\right] \tag{31}$$

where Ψ_s is the dimensionless liquid slug length L_S/d. Unfortunately, the basis for such a correlation remains unpublished. However, the authors compared the above correlation with that proposed by previous researchers (such as Eqs. 28, 30, and 31). The comparison shows that all the correlations more or less exhibit the same trend and are in the same range. However, the values predicted by Heiszwolf are slightly higher than those predicted by other researchers. The authors noted that the values predicted by Eq. 29 (Irandoust and Andersson, 1988a) were not in the range predicted by other correlations.

In a recent article Kreutzer et al. (2001) reported heat transfer studies using CFD simulation in a 1-mm-diameter tube and developed a correlation relating the Nusselt number (Nu) as a function of the dimensionless liquid slug length (Ψ_s), Reynolds number (Re), and Prandtl number (Pr) within the range $1 < \Psi_s < 16$, $7 < \mathrm{Pr} < 700$, and $10 < \mathrm{Re} < 400$. By analogy, the authors proposed the following correlation for the liquid–solid mass transfer coefficient

$$\mathrm{Sh} = 20\left[1 + 0.003\left(\frac{\Psi_s}{\mathrm{ReSc}}\right)^{-0.7}\right] \tag{32}$$

As is evident, most of the correlations are dependent on the liquid slug length. However, there is no method available to estimate the slug length *a priori*. The individual researchers have based their experimental results on their own observations of slug lengths, and may differ from one study to another.

Most of the experiments were conducted on a smooth surface and in clearly defined slugs of liquid. However, in an actual reactor, the liquid slugs may be aerated, giving rise to a "disturbance" on the liquid–solid interface. Moreover, monoliths likely to be used in industrial settings will seldom have smooth surfaces. These factors may cause deviations from model predictions (Nijhuis et al., 2001). Table 5 summarizes reported correlations for liquid–solid mass transfer coefficients.

Gas–liquid mass transfer

Gas–liquid mass transfer in nonstructured trickle-bed reactors has been studied in great detail by past researchers. Correlations that cover wide ranges of Reynolds number (Re) and Schmidt (Sc) numbers are available in the literature (for a review, see Ramachandran et al., 1983). Although the mechanism of transport is not expected to be significantly different in structured packing, the work in this field is somewhat limited and incoherent (Heiszwolf et al., 2001b).

Similar to their liquid–solid mass transfer work, Bercić et al. (1997) proposed a dimensional correlation for the gas–liquid mass transfer coefficient. Gas–liquid mass transfer coefficients were measured by physical absorption of methane in water, using capillary tubes of three different diameters (1.5, 2.5, and 3.1 mm). Methane and water formed the gas and liquid slugs, respectively. The measured data were fitted into the proposed expression, which was developed by assuming plug flow of the liquid slug and then using nonlinear regression as follows

$$k_{GL}a = \frac{0.111\,v^{1.19}}{[(1-\varepsilon_G)UCL]^{0.57}} \tag{33}$$

Because the expression does not contain any physical parameters of the gas and liquid used, it lacks generality and can be used only for methane–water systems. Heiszwolf et al. (1999) attempted to make the expression compatible with other systems by adding the following correction factor

$$(k_{GL}a)_A = (k_{GL}a)_B\left(\frac{D_A}{D_B}\right)^n \tag{34}$$

where n is the scaling factor: $n = 1$ for film theory, and $n = 0.5$ for penetration theory (Kreutzer et al., 2001). However, this modification has its own drawbacks and could not achieve the desired results (Heiszwolf et al., 1999).

In earlier work, Irandoust and Andersson (1988a) used the following correlation (Eq. 35) to compute k_{GL} as a needed parameter for modeling the overall performance of a monolith reactor. The authors cited unpublished work to support their claim

$$\mathrm{Sh} = 0.41\sqrt{\mathrm{ReSc}} \tag{35}$$

Table 5. Available Correlations for Liquid–Solid (L-S) and Gas–Liquid (G-L) Mass Transfer

Author (Year)	Correlation	
	Liquid–Solid Mass Tranfer	Gas–Liquid Mass Transfer
Hatziantoniou et al. (1982)	$\mathrm{Sh} = 3.51\left(\frac{\mathrm{ReSc}}{\gamma}\right)^{0.44}\beta^{-0.09}$ with $\gamma = L_c/d_c$ and $\beta = L_s/d_c$	
Irandoust et al. (1988a)	$\mathrm{Sh} = 1.5 \times 10^{-7}(\mathrm{Re})^{1.648}(\mathrm{Sc})^{0.177}(\alpha)^{-2.338}$ with $\alpha = \delta_f/d_c$	$\mathrm{Sh} = 0.41\sqrt{\mathrm{ReSc}}$
Irandoust et al. (1992)		$1 \le \mathrm{Re} \le 400$: $\frac{(\mathrm{Sh}-1)}{\mathrm{Sc}^{1/3}} = \left[1+\left(\frac{1}{\mathrm{ReSc}}\right)\right]^{1/3}\mathrm{Re}^{0.41}$ $100 \le \mathrm{Re} \le 2000$: $\mathrm{Sh} = 1 + 0.724\,\mathrm{Re}^{0.48}\mathrm{Sc}^{1/3}$
Bercić et al. (1997)	$k_{LS}a = \frac{0.069v^{0.63}}{[(1-\varepsilon_G)UCL - 0.105UCL\varepsilon_G]^{0.44}}$	$k_{GL}a = \frac{0.111v^{1.19}}{[(1-\varepsilon_G)UCL]^{0.57}}$
Heiszwolf et al. (1999)	$\mathrm{Sh} = 3.66\left[1+0.152\left(\frac{\Psi_s}{\mathrm{ReSc}}\right)^{-0.423}\right]$	$(k_{GL}a)_A = (k_{GL}a)_B\left(\frac{D_A}{D_B}\right)^n$ $n = 1.0$ for film theory $n = 0.5$ for penetration theory (Kreutzer et al., 2001)
Lebens et al. (1999a)		$\mathrm{Sh} = 1.04 + \frac{0.093\zeta^{-0.87}}{1+0.047\zeta^{-0.61}}$ with $\zeta = \frac{L_cD_L}{d_{fM}^2u_{LM}}$
Kreutzer et al. (2001)	$\mathrm{Sh} = 20\left[1+0.003\left(\frac{\Psi_s}{\mathrm{ReSc}}\right)^{-0.7}\right]$	

In a more recent paper, Irandoust et al. (1992) assumed the hemispherical caps of the gas bubble to be rigid spheres and cited previous literature on mass transfer correlations for rigid spheres to propose the following gas–liquid mass transfer coefficient

$$1 \le \mathrm{Re} \le 400: \quad \frac{(\mathrm{Sh}-1)}{\mathrm{Sc}^{1/3}} = \left[1+\left(\frac{1}{\mathrm{ReSc}}\right)\right]^{1/3}\mathrm{Re}^{0.41} \tag{36}$$

$$100 \le \mathrm{Re} \le 2000: \quad \mathrm{Sh} = 1 + 0.724\,\mathrm{Re}^{0.48}\mathrm{Sc}^{1/3} \tag{37}$$

Irandoust et al. (1992) performed the experiments in a single capillary tube with three different liquids: water, ethanol, and ethylene glycol. Air and the liquid were passed cocurrently upward, and the outlet concentration of oxygen in the liquid was measured for model validation. However, the model overestimated the experimental results by about 30% and therefore Eq. 37 should be multiplied by a factor of 0.686 before it is used elsewhere.

During the last decade, processes with two-phase cocurrent upward or downward flow have been well investigated in monolith reactors. Different researchers have provided a variety of experimental and theoretical data. Recently a new type of structure, the internal finned reactor, was presented by Lebens et al. (1997). This structure enables countercurrent operation in the monolith. The monolith reactor operates in the annular flow regime, and the fins help to stabilize the liquid film flow. The mechanism of mass transfer is therefore significantly different from monoliths operated in the slug-flow regime.

Lebens et al. (1999a) reported both experimental and predicted results on data for gas–liquid mass transfer coefficients. In the experiment, the gas–liquid mass transfer coefficient was determined by measuring desorption by nitrogen gas flow of oxygen from oxygen saturated water. The authors also developed a correlation by solving the convection–diffusion equation for a smooth laminar falling liquid film flow on a vertical plane, as follows

$$\mathrm{Sh} = 1.04 + \frac{0.093\zeta^{-0.87}}{1+0.047\zeta^{-0.61}} \tag{38}$$

with

$$\zeta = \frac{L_cD_L}{\delta_{f,m}^2u_{L,m}} \tag{39}$$

where L_c is the tube length, D_L is the diffusivity, $\delta_{f,m}$ is the maximum film thickness, and $u_{L,m}$ is the maximum liquid velocity.

It must be noted that the Sherwood number is a function of the dimensionless tube length (ζ), and for higher values of ζ it approaches the asymptotic value of 1.04. The experimental values in general had good agreement with the above correlation (Eq. 38), except at the inlet region of the tube, where the correlation underestimates the experimental values by a wide margin.

The area of contact for gas–liquid mass transfer has always been evaluated by assuming hemispherical plugs. However, in reality, the shape is more complex and varies with capillary number (Cybulski and Moulijn, 1998).

Despite all the work performed to develop mass transfer correlations, they have yet to be used effectively in models of monolith reactor performance at pilot plant or industrial scales. Nijhuis et al. (2001) used the mass transfer correlation devel-

oped by Irandoust et al. (1992) to model a pilot scale reactor. However, the reactor performance predicted by the model far overestimated the actual performance in experiments. The authors argue that in actual reactors the resistance layer is much thicker than that in model assumptions. Moreover, the washcoated channel walls are irregular, which would contribute to the increase in mass transfer resistance.

As mentioned in the previous section, aeration of the slug may introduce error in operation near the churn flow regime. A comprehensive study is needed to account for all of these factors, so that the correlations can be used in overall modeling with some degree of confidence. Table 5, found at the end of this section, lists the available correlations for liquid–solid and gas–liquid mass transfer coefficients.

Gas–solid mass transfer

Researchers have evaluated the gas–solid mass transfer in a simplistic manner. The gaseous reactant diffuses to the solid surface through the thin film surrounding the gas slug. The thin-film model was therefore used to determine the gas–solid mass transfer coefficient (Cybulski et al., 1993; Edvinsson et al., 1994; Irandoust et al., 1988)

$$k_{G\text{-}S} = \frac{D}{\delta_f} \tag{40}$$

Therefore, to determine the gas–solid mass transfer coefficient, one has to evaluate the film thickness (δ_f) of the liquid film, which depends primarily on the surface tension of the liquid and the liquid diffusivity (D). However, the film thickness is not uniform around the periphery of the monolith channel, and a mechanism to account for this nonuniformity needs to be designed. It must be noted that experiments to directly determine the gas–solid mass transfer coefficient are not available in the literature.

Reactor Performance

So far we have dealt with the hydrodynamics and the transports inside monolith packing being operated in a range of operating conditions. These studies help us to understand the basic characteristics of monolith packing under cold flow conditions—with no chemical reactions. Many unit operations, such as absorption, stripping, and distillation, can be modeled better with these basic understandings.

The primary objective of this work is to review the effectiveness of monoliths for gas–liquid–solid reactions. Currently, the conventional reactors, such as slurry, fluidized-bed, and packed-bed reactors have been used in industry to carry out three-phase reactions. For a decade now, researchers have shown that structured packing could be a viable alternative to that for mass transfer limited reactions. However, to effectively compete with conventional reactors, a wide range of reactions need to be studied in structured packing, and an adequate model to predict performance also needs to be devised.

This section covers work on these topics by various researchers. It includes investigations of different test chemical reactions (see the following subsection). The reactions were chosen for their industrial relevance or for being intrinsically fast or slow. Although it is well known that monolith structures favor fast reactions, studies of intrinsic slow reactions also help gauge the effectiveness of the monolith.

Most of the researchers, while evaluating the performance of monolith, have compared it with that of conventional reactors. There has been a general disagreement about the basis on which such comparison should be made, as discussed in the section on performance comparison. Finally, the models proposed by investigators are outlined in the section on reactor modeling. These models are based on the mass balance of the reacting species, taking into account different mass transport phenomena occurring inside the packing.

Test chemical reactions used

Monolith reactors have primarily been used to catalyze automobile engine exhaust. More recently, multiphase reactions such as hydrogenation, and partial and complete oxidation reactions, which are traditionally performed in slurry, fluidized, or packed-bed reactors, are being tried in structured packing, such as monoliths, sandwich or open cross-flow structures, and foam structures.

The advantages of structured packing lie in the field of fast reactions, which are mass transfer limited. The intense mixing in the segmented slug flow, together with the very thin liquid film between the gas bubbles and the catalyst surface, leads to enhanced mass transfer. In studying the overall performance of monolith reactors, the researchers have chosen a particular reaction for a variety of reasons. Some reactions represent industrially relevant processes or exemplify a group of similar reactions; other reactions have well-known kinetics and substantial amounts of experimental and theoretical data available.

Most of the research efforts has centered on hydrogenation reactions, one of the most important reactions in the petroleum and fine chemical industries. These reactions are typically a three-phase reaction over a catalyst surface, in which hydrogen reacts with liquid in the presence of a solvent, which improves heat removal. Another type of reaction, catalytic wet oxidation, can be used to purify industrial and human wastewater. Such processes are characterized by the reaction of oxidizable liquid or solid with a gaseous source of oxygen, such as air or pure oxygen, to produce CO_2 and other innocuous end products (Mishra, 1995). Table 6 gives a summary of research performed using test reactions in monolith beds. As the table suggests, most reactions studied in monolith reactors are either hydrogenation or oxidation reactions, which are normally intrinsically fast reactions. This is the type of reactions monolith is most suited for, given that enhancing mass transfer is what it does best. It cannot enhance the intrinsic rate. On certain occasions, very slow reactions have also been studied, to compare the intrinsic reaction rate and overall reaction rate in a monolith reactor.

Performance comparison between monolith and conventional reactors

The focus of most investigations of monolith and other structured packing for three-phase reactors is to evaluate their performance vs. traditional reactors such as slurry bubble columns, trickle-bed reactors, and batch reactors. Comparison has been made both experimentally and by using model predictions. Table 7 provides a summary of the comparison studies. Frequently, the basis of comparison is the extent of conversion

Table 6. Summary of Reported Investigations Performed Using Test Reactions in Monolith Beds

Author	Reaction	Catalyst/Support	Conditions	Velocities/Mode of Operation
Hatziantoniou et al. (1984)	Hydrogenation of nitrobenzoic acid	2.5 wt % Pd	310, 353 K 1, 4 bar	u_{tot} = 3.03–5.1 *cm/s downflow*
Hatziantoniou (1986)	Hydrogenation of nitrobenzene and *m*-nitrotoluene	5.4 wt % Pd SiO_2	246, 376 K 5.9, 9.8 bar	u_{tot} = 1.7–4.2 *cm/s downflow*
Mazzaroni (1987)	Hydrogenation of α-methylstyrene	1 wt % Pd	303–323 K 0.2–1 bar	u_L = 0.05–0.34 cm/s u_G up to 0.12 cm/s upflow, downflow
Irandoust (1988a)	Hydrogenation of 2-ethylhexenal	0.5 wt % Pd SiO_2	413, 433 K 4.0, 9.8 bar	u_{tot} = 2.3–8.5 cm/s downflow
Kawakami (1989)	Oxidation of glucose	Glucose oxidase	298 K	u_L = 0.004–0.25 cm/s u_G = 0.5–6.0 cm/s upflow, downflow
Irandoust (1990)	Hydrodesulfurization of thiophene and hydrogenation of cyclohexene	12 wt % Co 4 wt % Mo γ-Al_2O_3	509, 523 K 30, 40 bar	u_{tot} = 1.72–2.13 cm/s downflow
Edvinsson (1993)	Hydrodesulfurization of dibenzothiophene	C–Mo γ-Al_2O_3	543, 558, 573 K 60, 70, 80 bar	u_{tot} = 4.6 cm/s downflow
Edvinsson (1995)	Hydrogenation of acetylene	0.04 wt % Pd α-Al_2O_3 γ-Al_2O_3	303, 313 K 13, 20 bar	u_L = 0.66 cm/s u_G = 6.5 cm/s downflow
Crynes (1995)	Oxidation of aqueous phenol	CuO γ-Al_2O_3	383–423 K 4.8–11.7 bar	u_L = 0.4–3.5 cm/s u_G = 15.8–50 cm/s upflow
Smits (1996)	Hydrogenation of a mixture of styrene and 1-octane in toluene	Pd α-Al_2O_3	316, 343 K 5–15 bar	u_{tot} = 5.0–45.0 cm/s downflow
Klinghoffer (1998a,b)	Wet oxidation of acetic acid	Pt Al_2O_3	385–573 K 3.5–128 hour	u_L = 0.024–0.093 cm/s u_G = 2.36 cm/s (SCM) upflow
Patrick (2000)	Wet oxidation of glucose and cellulose	0.26 wt % Pt Al_2O_3	333–455 K	u_L = 0.024 cm/s u_G = 1.48 cm/s (SCM) upflow
Nujhuis (2001)	Hydrogenation of α-methylstyrene hydrogenation of benzaldehyde	1 wt % Ni 9 wt % γ-Al_2O_3	373, 423 K 10, 15 bar	u_{tot} = 20 cm/s downflow
Schutt (2002)	Wet oxidation of cellulose	0.34 wt % Pd Al_2O_3	373–428 K	u_L = 0.026 cm/s u_G = 2.2 cm/s (SCM) upflow
Liu (2002)	Dehydrogenation of ethylbenzene	72 wt % α-Fe_2O_3 16 wt % K2O 4 wt % CeO_2	866, 878 K 1 bar	u_L = 0.0014 cm/s downflow

under similar operating conditions, productivity, selectivity, and pressure drop. The volume of catalyst was the primary weighting factor for comparison of different reactors. However, the mass of catalyst, mass of active metal, and external surface area have also been considered in the comparisons.

Compared to the conventional reactors, structured packing

Table 7. Summary of Studies on the Comparisons between Monolith and Conventional Reactors

Author	Comparison	Kind of Study	Reaction
Mazzaroni et al. (1987)	Monolithic reactor vs. trickle-bed reactor	Experimnental studies	Hydrogenation of α-methylstyrene
Cybulski et al. (1993)	Monolithic reactor vs. literature data of slurry columns, autoclaves, and trickle-bed reactors	Mathematical model of monolith reactor	Liquid-phase methanol synthesis
Edvinsson et al. (1994)	Monolithic reactor vs. trickle bed	Numerical simulations	Three-phase hydrogenation
Cybulski et al. (1999)	Monolithic reactor vs. agitated-slurry reactor	Mathematical modeling of both reactors	Hydrogenation of 3-hydroxypropanal
Nijhuis et al. (2001)	Monolithic reactor vs. trickle-bed reactor	Pilot-scale study	Hydrogenation of α-methylstyrene and benzaldehyde
Stankiewicz et al. (2001)	In-line monolith reactor vs. trickle-bed reactor	Theoretical studies	
Heiszwolf et al. (2001a)	Monolith loop reactor vs. bubble column and slurry reactor	Theoretical studies	
Roy (2002)	Generic method to design monolith catalyst Monolith reactor vs. pellet-based trickle-bed reactor	Theoretical studies	

leads to differences in catalyst loading, mass transfer resistance, contacting area, and pressure drop because of the regularity. There is no doubt that the new structures have a superior advantage with respect to pressure drop. The other parameters, however, have to be investigated further and optimized to guarantee a better overall performance than that of traditional reactors. Unfortunately, various investigators have used different criteria for the comparison of monoliths with traditional reactors.

Mazzarino and Baldi (1987) investigated hydrogenation of α-methylstyrene into cumene using a ceramic monolith coated with Pd. Comparison was made with a trickle-bed reactor (TBR) based on catalyst weight, and the monolith reactor was found to perform better than the TBR at high gas flow rates, whereas the reaction rate was virtually insensitive to the liquid flow rate. The monolith performed better in upflow mode than in downflow mode because of better wetting of the catalyst. Figure 8 shows the hydrogenation rates per unit Pd mass of α-methylstyrene in the monolith reactor and the TBR at different gas flow rates under the same operating conditions. It should be noted that better mass transfer in monolith is attributed to recirculation within the liquid slugs and to the thin liquid film separating the gas slug from the catalyst layer, as mentioned earlier. To demonstrate this point, the authors conducted a single-phase reaction, in which the liquid was saturated with hydrogen before entering the reactor. In this circumstance the TBR performed better than monolith in terms of overall conversion.

Cybulski et al. (1993) developed a mathematical model for liquid-phase methanol synthesis. Different process conditions and design parameters were simulated. It was found that the optimum thickness of the catalyst layer is in the range of 50–75 μm. The authors found that the performance of a monolith reactor is not always superior to that of a conventional reactor. The monolith reactor's performance was better with respect to CO conversion and methanol productivity per unit volume of the reactor when a stoichiometrically balanced syngas was used as feed. The improvement stems from the fact that the monolith reactor used contained a theoretically higher concentration of catalyst than did the slurry reactor. In the case of the TBR, even though the catalyst concentration is higher, the intraparticle diffusional resistance is significantly higher.

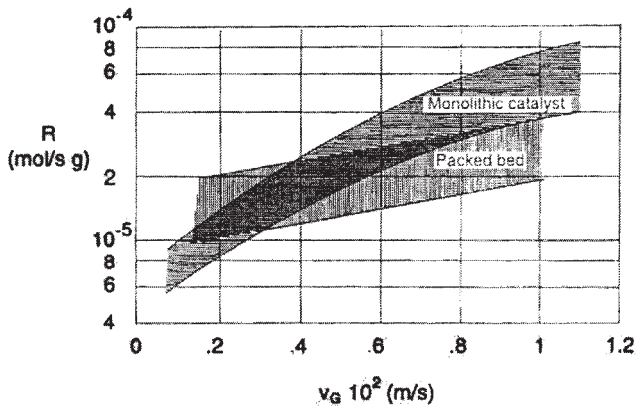

Figure 8. Conversion rates per unit palladium mass of hydrogenation of α-methyl styrene vs. gas velocity at 313 K (from Mazzarino et al. (1987).

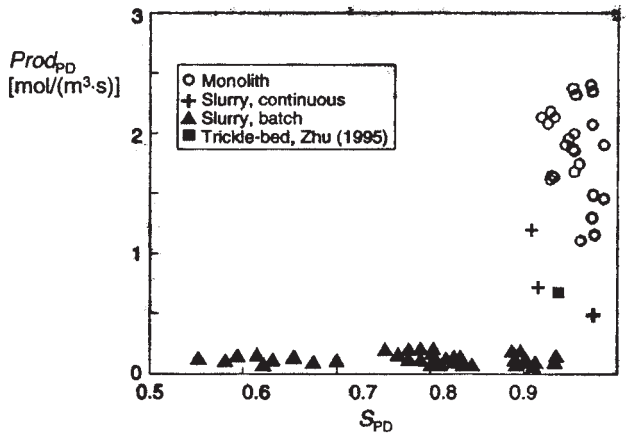

Figure 9. Attainable selectivity and production for MASR, MR, and TBR (from Cybulsky et al., 1999).

Edvinsson et al. (1994) used numerical simulation to quantitatively compare the performance of a conventional trickle-bed reactor and a monolith reactor, based on the catalyst load. The monolith reactor had washcoated catalyst with varying washcoat thickness (resulting in catalyst fraction between 6 and 33%), whereas catalyst particles used in the simulated TBR had eggshell with a thickness corresponding to approximately the same catalyst loading (t_{shell} values of 0.5 to 0.05d_p). The model reaction was a consecutive three-phase hydrogenation. For the model system, the selectivity of the intermediate product was found to be higher for the monolith over almost the whole range of variables studied. For particles larger than 2 mm, the volumetric space–time yield was higher in the monolith reactor compared to that in the TBR. For particles smaller than 2 mm, however, the pressure drop in the TBR is considerably higher. The pressure drop in the MR was sufficiently low that gas could be recirculated without the requirement of external pumping.

Cybulski et al. (1999) conducted a comparative study of hydrogenation of 3-hydroxypropanal to 1,3-propanediol in a mechanically agitated slurry reactor (MASR) and a monolith reactor. A purely numerical study was done to compare the performance of the MR and MASR based on productivity (mol/m^3 s^{-1}) and selectivity. Although the comparisons were made on the basis of per unit reactor volumes, the authors emphasized the point that much more catalyst can be packed in an MR than in an MASR per unit volume. They adopted a modeling approach similar to that used by Edvinsson et al. (1994), discussed earlier. Intrinsic kinetics, mass transfer correlations, and model equations derived earlier by various researchers (Andersson, 1998; Zhu, 1995) were directly used in this study. As shown in Figure 9, the numerical studies clearly demonstrated the superior performance of the MR over MASR, with respect to reactor productivity and process selectivity.

It should be noted that the actual productivity of a MASR is higher than that shown in the figure. However, given that an MASR requires considerable downtime for filling, emptying, and filtering, the overall productivity decreases significantly.

Nijhuis et al. (2001) did a comparative study of hydrogenation of α-methylstyrene and benzaldehyde in a trickle-bed reactor and a monolith. Experimental results showed that the

monolith reactor had a 50% higher activity per unit reactor volume than that of the trickle-bed reactor (Table 8), even though the porosity of the monolith reactor is relatively high—this despite the fact that the intrinsic rate for the extruded catalyst used in the TBR was slightly more than that of the MR catalyst. This finding clearly demonstrates the fact that the better performance in the MR is entirely attributed to its structure. Experiments also revealed that the enhanced MR performance resulted from the fact that Taylor bubbles in an MR form a thin film through which most of the mass transfer takes place. If, instead, the liquid reactant is saturated with hydrogen and the resultant single phase is passed through the MR, the activity falls to about one fourth of the three-phase Taylor flow regime.

MRs are also known to exhibit higher selectivity because of the narrow distribution of their residence time. The hydrogenation of benzaldehyde showed significantly higher selectivity (>90%) with respect to benzylalcohol in an MR, whereas a TBR gave a selectivity of 73%, thus reaffirming the advantage of the MR over the TBR.

Stankiewicz (2001) proposed a novel concept in which the conventional reactor vessel is replaced with monolith units, installed in the process pipelines. The reactor configuration is known as an "in-line monolith reactor" (ILMR). The author made comparison studies for a slow hydrogenation reaction ($k = 3.94 \times 10^{-3}$ m^3_{liquid} s^{-1} $kg_{catalyst}$) in a monolith and trickle-bed reactor with 3.5-mm impregnated catalyst particles. The monolith was assumed to be operated purely in liquid phase, the feed being saturated with hydrogen, much in excess of stoichiometric proportions. To achieve 95% conversation of the limiting reactant, the simulation results showed that for a cell density ranging from 200 to 1100 cpsi and a washcoat thickness of 17–70 μm, the required reactor volume is 6 to 53 times less than that of a conventional trickle-bed reactor. The author also compared the performance of different cell densities and washcoat thicknesses and found that the required monolith reactor volume increased with increasing washcoat thickness and cell density.

Heiszwolf et al. (2001) used the conventional way of comparing the performance of different types of conventional reactors, while studying the hydrodynamic aspects of a monolith loop reactor. The authors used the power input per unit volume of the system (P/V) to obtain a certain gas–liquid mass transfer rate as the indicator for reactor performance. The P/V for monolith reactor was calculated using the following expression

$$\frac{P}{V} = \frac{\Delta P_L \varepsilon u_L}{L} \tag{41}$$

Table 8. Bed Characteristics Used in Comparing the Performance of a Monolith and TBR Using Mass Transfer Limited Hydrogenation of α-Methylstyrene over an Eggshell Nickel Catalyst*

Activity per Parameter	Unit	Monolith (400 cpsi)	Trickle Bed
Reactor volume	$mol/m^3_{reactor}/s$	6.2	4.6
Geometrical surface area	$mol/m^2_{geom}/s$	1.9×10^{-3}	2.0×10^{-3}
Catalyst amount	$mol/g_{catalyst}/s$	1.1×10^{-5}	6.2×10^{-5}
Nickel amount	$mol/g_{nickel}/s$	9.8×10^{-4}	8.4×10^{-5}

*Conditions: 373 K, 10 bar H_2 (from Nijhuis et al., 2001).

For stirred tanks and bubble columns, previously reported correlations for P/V were used (Schluter et al., 1992; van't Riet, 1979). For low P/V, It was found that the $k_{GL}a$ value for the monolith configuration was much higher than that for other conventional reactors. For high P/V (>10,000 W/m^3), all types of reactor give comparable $k_{GL}a$ values. It was further observed that for monolith reactors, the $k_{GL}a$ value is a weak function of P/V, meaning the mass transfer coefficient remains almost constant for significantly high gas and liquid flow rates.

Reactor modeling

Because of its well-defined structure, the modeling of monolith is considered more straightforward than the modeling of random packed beds. However, the environment outside the monolith (distributor, outlet arrangements) affects its performance to a great extent. This section deals with different models reported in the literature to simulate the performance of monolith reactors. In most published work related to monolith, maximum emphasis has been given to mass transfer correlations and pressure drop because these packings have been used in industry for over two decades as mass transfer elements, such as in distillation and absorption.

Table 9 lists the models for monolith reactors reported in the literature. Three distinct reactor models for monolith reactors have been published in the open literature. Hatziantoniou et al. (1984) and Irandoust et al. (1988a) proposed models for monolith reactors operating in the Taylor flow regime. The one proposed by Irandoust gained more attention and was subsequently used by other researchers (Edvinsson et al., 1994; Stankiewicz et al., 2001). More recently, Liu et al. (2002) and Roy et al. (2002) dealt with monolith reactors operated in the film-flow regime, which is more akin to the trickle-flow regime in packed beds. In the model developed by Irandoust et al. (1988), and later adopted by Edvinsson et al. (1994) and others, plug flow was assumed in the liquid phase. Three different mass transfer fluxes were considered in the differential mass balance for reacting species, as shown in Figure 10.

In all the studies involving this model, a good agreement was observed between experimental studies (Irandoust et al., 1988) and a superior performance compared to trickle-bed reactor (TBR). However, Nijhuis et al. (2001) reported experimentally determined activity of monolith per unit volume severalfold lower compared to that predicted by using the model. The authors cited reasons including irregular wall structure and nonuniform liquid film thickness, both contributing to lower mass transfer rate in the experiment. Several other factors that could affect the performance of monolith are aeration of liquid slugs (Mewes et al., 1999), irregular liquid and gas slug length (Sederman et al., 2003), initial maldistribution of gas and liquid reactants (Reinecke et al., 1996), and compression of gas slugs. Important parameters for monolith reactor modeling, phase holdup, and contact surface area for mass transfer depend on these factors. A detailed study of these hydrodynamic effects is the current need. Carefully executed experiments and a detailed computation fluid dynamic (CFD) study could help us to better understand the occurring phenomena.

Hatziantoniou et al. (1984) modeled hydrogenation of nitrobenzoic acid (NBA) in a monolith reactor. The model was simplified by the fact that the intrinsic reaction rate was zero order with respect to NBA, and first order with respect to

Table 9. Summary of Overall Reactor Models Available in the Literature

Author	Flow Regimes	Basic Approach	Design Equation in the Bulk	Interface Equations	Hydrodynamic Equations
Edvinsson et al., 1994	Gas–liquid slug flow	Three distinct mass transfer rates, plug flow in each phase	$\frac{d}{dz}\begin{bmatrix}F_G\\F_L\end{bmatrix}=\begin{bmatrix}-N_{GL}-N_{GS}\\N_{GL}-N_{LS}\end{bmatrix}$	Interface between	Plug flow in both gas and liquid slugs, no slip between gas and liquid slugs
			Refer to Figure 10	Gas/liquid $N_{GL,i}=(k_{GL}a)_i\left(\frac{P_i}{He_i}-c_{L,i}\right)$	
				Liquid/solid $N_{LS,i}=(k_{LS}a)_i(c_{L,i}-c_{s,i})=f_w x_{cat}\sum_j \nu_{i,j}\eta_j r_{L,j}$	
				Gas/solid $N_{GS,i}=(k_{GS}a)_i(c_{I,i}-c_{s,i})=(1-f_w)x_{cat}\sum_j \nu_{i,j}\eta_j r_{I,j}$	
Roy et al., 2002	Annular flow (gas core/liquid film)		$u_{L0}\frac{dc}{dz}=-r_{app}$	Within washcoat (to calculate catalyst effectiveness, η_e	Gas core/liquid film (annular) regime. Both liquid and gas under laminar flow with no slip at the interface.
			$r_{app}=\gamma_e\eta_i(1-OFA)r_{cat,v}$	$\nabla(D_e\nabla c_s)=r_{cat,v}$; $c_s=c_{bulk}$ at S-L interface $\nabla c_s=0$ at the plane of symmetry within the solid wall Within liquid $u_{L,z}\frac{\partial c}{\partial z}=\nabla(D\nabla c)$	

hydrogen. This model differs from the model proposed by Irandoust et al. (1988) only in that the primary mass balance of hydrogen was carried out inside the washcoat as an unsteady-state diffusion–reaction problem, instead of in the channel. The transport phenomena in the channels acted as boundary conditions for the design equation. Unfortunately, the model also contains liquid and gas slug time constants, which cannot be known *a priori* without doing actual experiments. For this reason, and also because of the model's inability to incorporate more complex reaction rate forms, it has not gained favor in subsequent years, and therefore is not included in Table 9.

Roy et al. (2002) published a part of their work on reactor modeling of monolith reactors working in the film-flow regime. The authors aimed to develop criteria to determine the optimum design (washcoat thickness, channel diameter) of a monolith based on the intrinsic kinetic rate of reactions. The film-flow regime is achieved when the reactor is operated at very low liquid velocity (0.1 to 2 cm/s), similar to trickle flow in a packed-bed reactor. The authors proposed three levels of modeling. A one-dimensional, plug-flow, steady-state, convection–reaction equation was advanced to describe the annular film. It gives the concentration profile of the reacting species along the length of the reactor. Two extra parameters, the velocity profile in the film and the effectiveness factor arising out of diffusion resistance inside the catalyst, are needed to solve the above equation. They were modeled separately. To obtain the effectiveness factor, the standard equation for slab geometry $\eta = \tan\phi/\phi$ was used. The Thiele modulus $\phi = l\sqrt{(k/\mathbf{D})}$ was found to be adequate for all shapes when the diffusion length scale "l" was expressed as $l = (1 - OFA)/GSA$. For each velocity, the velocity profile inside the film was solved using the standard Navier–Stokes equation.

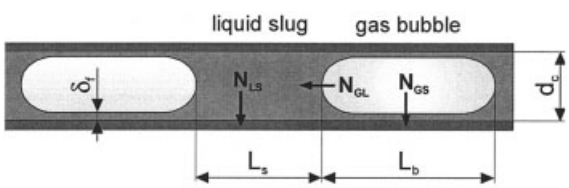

Figure 10. Different mass transfer fluxes used in the monolith reactor modeling of Irandoust et al. (1989) and Edvinsson et al. (1994).

The results show that for slow reactions a monolith with high solid fraction is preferred because the higher diffusion resistance does not have a strong bearing and more catalyst can be packed in a unit volume. For fast reactions, optima exist with respect to the diffusion length, and any further increase in catalyst wall thickness decreases the volumetric activity.

This latest study heralds a new question in the research pertaining to monoliths. To date, slug flow has been advocated as being the most advantageous flow regime. A comparison of monolith performance operating in slug-flow and film-flow regions is in order.

Acknowledgments

The authors gratefully acknowledge the financial support provided by Bayer Technology Services, Bayer AG, Germany.

Notation

a = interfacial area per unit volume, 1/L
C = factor
C = distribution parameter
$cpsi$ = cells (or channels) per square inch
D = diffusion coefficient, m^2/s
d_b = bubble diameter
d_c = capillary diameter
d_h = hydraulic diameter m
d_P = dispersed bubble diameter, m
dp/dz = pressure gradient, Pa/m
D_R = reactor diameter, m
F = factor
f = friction factor
g = gravity, m/s^2
GSA = geometric surface area, $in.^2/in.^3$
k = mass transfer coefficient, m/s
L = length, m
L = cell spacing, in.
L_b = gas bubble length, m
$L_{b\ =\ \text{constant bubble length}}$ (d_c = 2 mm), m
L_c = channel length
L_R = reactor length, m
L_s = liquid slug length, m
MR = monolith reactor
n = cell density, cpsi
OFA = open frontal area
P/V = power input per unit volume of the system, W/m^3
R = radius of the capillary, m
R = radius of gas plug, m
Re = Reynolds number = $vd\rho/\mu$
Sc = Schmidt number = $\mu\rho/D$
Sh = Sherwood number = kd/D
t = wall thickness, mm
TBR = trickle-bed reactor
UCL = unit cell length = $L_b + L_s$
u_G = superficial gas velocity, m/s
u_L = superficial liquid velocity, m/s
$u_{L,m}$ = maximum liquid velocity, m/s
u_{tot} = sum of superficial gas and liquid velocity ($u_L + u_G$), m/s
V = volume, m^3
v = cell velocity, m/s
v_b = bubble velocity, m/s
v_G = gas velocity, m/s
$V_{G,u}$ = drift velocity, m/s
We = Weber number = $\rho_l v_l^2 d_p/\sigma$
x = quality
Δp = pressure drop
$\Delta P/\Delta L$ = pressure drop per unit length, Pa/m
ΔP_G = pressure drop caused by gas, Pa

Greek letters

α = dimensionless film thickness = δ_f/d_t
Φ = volumetric flow rate, m^3/s
Ψ_s = liquid slug length, m
δ_f = liquid film thickness, m
$\delta_{f,m}$ = maximum film thickness, m
ε = bed void fraction
ε_G, β = gas holdup
ε_{gG} = volume fraction of bubbles
$\varepsilon_{gG/Lb}$ = number of bubbles per unit length
ε_L = liquid holdup
$\gamma = L_c/d_c$
μ = dynamic viscosity, kg/ms
ρ = density, kg/m^3
σ = surface tension, N/m
ζ = dimensionless tube length

Subscripts

A = species A
B = species B
b = bubble
c = capillary, channel
D = Darcy
F = Fanning
fr, f = frictional
g = gas
G = gas
GL = gas–liquid
GS = gas–solid
h = hydraulic
l = liquid
L = liquid
LF = liquid film alongside a Taylor bubble
LS = liquid–solid
m = measured
$orif$ = orifice
P = dispersed bubble
R = reactor
s = slug
st = hydrostatic
tot = total
TP = two phase
z = length

Superscripts

* = dimensionless velocity
n = scaling factor

Literature Cited

Albers, R. E., M. Nyström, M. Siverström, A. Sellin, A. C. Dellve, U. Andersson, H. Herrmann, and Th. Berglin, "Development of Monolith Based Process for H_2O_2 Production: From Idea to Large-Scale Implementation," *Catal. Today*, **69**, 247 (2001).

Al-Dahhan, M. H., and W. Highfill, "Liquid Holdup Measurement Techniques in Laboratory High Pressure Trickle Bed Reactors," *Can. J. Chem. Eng.*, **77**(4), 759 (1999).

Al-Dahhan, M. H., F. Larachi, M. P. Dudukovic, and A. Laurent, "High-Pressure Trickle-Bed Reactors: A Review," *Ind. Eng. Chem. Res.*, **36**(8), 3292 (1997).

Andersson, B., S. Irandoust, and A. Cybulski, "Modeling of Monolith Reactors in Three-Phase Processes," *Chem. Ind. Struct. Catal. & Reactors* (Dekker), **71**, 267 (1998).

Bercić, G., and A. Pintar, "The Role of Gas Bubbles and Liquid Slug Lengths on Mass Transport in the Taylor Flow through Capillaries," *Chem. Eng. Sci.*, **52**(21–22), 3709 (1997).

Biswas, J., and P. F. Greenfield, "Two-Phase Flow through Vertical Capillaries—Existence of a Stratified Flow Pattern," *Int. J. Multiphase Flow*, **11**(4), 553 (1985).

Boyer, C., and B. Fanget, "Measurement of Liquid Flow Distribution in Trickle Bed Reactor of Large Diameter with a New Gamma-Ray Tomographic System," *Chem. Eng. Sci.*, **57**, 1079 (2002).

Broekhuis, R. R., R. M. Machado, and A. F. Nordquist, "The Ejector-Driven Monolith Loop Reactor—Experiments and Modeling," *Catal. Today*, **69**(1–4), 87 (2001).

Chen, J., R. Novica, M. H. Al-Dahhan, and M. P. Dudukovic, "Study of Particle Motion in Packed/Ebullated Beds by Computed Tomography (CT) and Computer Automated Radioactive Particle Tracking (CARPT)," *AIChE J.*, **47**(5), 994 (2001).

Coleman, J. W., and S. Garimella, "Characterization of Two-Phase Flow Patterns in Small Diameter Round and Rectangular Tubes," *Int. J. Heat Mass Transfer*, **42**(15), 2869 (1999).

Crynes, L. L., R. L. Cerro, and M. A. Abraham, "Monolith Froth Reactor: Development of a Novel Three-Phase Catalytic System," *AIChE J.*, **41**(2), 337–45 (1995).

Cybulski, A., R. Edvinsson, S. Irandoust, and B. Andersson, "Liquid-Phase Methanol Synthesis: Modelling of a Monolithic Reactor," *Chem. Eng. Sci.*, **48**(20), 3463 (1993).

Cybulski, A., and J. A. Moulijn, *Structured Catalysts and Reactors*, Marcel Dekker, New York (1998).

Cybulski, A., A. Stankiewicz, R. K. Edvinsson Albers, and J. A. Moulijn, "Monolithic Reactors for Fine Chemicals Industries: A Comparative

Analysis of a Monolithic Reactor and a Mechanically Agitated Slurry Reactor," *Chem. Eng. Sci.*, **54**(13–14), 2351 (1999).
Edvinsson, R. K., and A. Cybulski, "A Comparative Analysis of the Trickle-Bed and the Monolithic Reactor for Three-Phase Hydrogenations," *Chem. Eng. Sci.*, **49**(24), 5653 (1994).
Edvinsson, R. K., A. M. Holmgren, and S. Irandoust, "Liquid-Phase Hydrogenation of Acetylene in a Monolithic Catalyst Reactor," *Ind. Eng. Chem. Res.*, **34**(1), 94 (1995).
Edvinsson, R. K., M. J. J. Houterman, T. Vergunst, E. Grolman, and J. A. Moulijn, "Novel Monolithic Stirred Reactor," *AIChE J.*, **44**(11), 2459 (1998).
Edvinsson, R. K., and S. Irandoust, "Hydrodesulfurization of Dibenzothiophene in a Monolithic Catalyst Reactor," *Ind. Eng. Chem. Res.*, **32**(2), 391 (1993).
Ellenberger, J., and R. Krishna, "Counter-Current Operation of Structured Catalytically Packed Distillation Columns: Pressure Drop, Holdup and Mixing," *Chem. Eng. Sci.*, **54**(10), 1339 (1999).
Folger, H. S., *Elements of Chemical Reaction Engineering*, Prentice Hall, Englewood Cliffs, NJ (1992).
Froment, G. B., and K. B. Bischoff, *Chemical Reactor Analysis and Design*, Wiley, New York (1990).
Garcia-Bordeje, E., F. Kapteijn, and J. A. Moulijn, "Preparation and Characterisation of Carbon-Coated Monoliths for Catalyst Supports," *Carbon*, **40**(7), 1079 (2002).
Gulati, S. T., "Ceramic Catalyst Supports for Gasoline Fuel," *Structured Catalysts and Reactors*, A. Cybulski and J. A. Moulijn, eds., Marcel Dekker, New York, pp. 15–58 (1998).
Harter, I., C. Boyer, L. Raynal, G. Ferschneider, and T. Gauthier, "Flow Distribution Studies Applied to Deep Hydro-Desulfurization," *Ind. Eng. Chem. Res.*, **40**(23), 5262 (2001).
Hatziantoniou, V., and B. Andersson, "Solid–Liquid Mass Transfer in Segmented Gas–Liquid Flow through a Capillary," *Ind. Eng. Chem. Fundam.*, **21**(4), 451 (1982).
Hatziantoniou, V., and B. Andersson, "The Segmented Two-Phase Flow Monolithic Catalyst Reactor. An Alternative for Liquid-Phase Hydrogenations," *Ind. Eng. Chem. Fundam.*, **23**(1), 82 (1984).
Hatziantoniou, V., B. Andersson, and N. H. Schoon, "Mass Transfer and Selectivity in Liquid-Phase Hydrogenation of Nitro Compounds in a Monolithic Catalyst Reactor with Segmented Gas–Liquid Flow," *Ind. Eng. Chem. Proc. Des. Dev.*, **25**(4), 964 (1986).
Heibel, A. K., J. J. Heiszwolf, F. Kapteijn, and J. A. Moulijn, "Influence of Channel Geometry on Hydrodynamics and Mass Transfer in the Monolith Film Flow Reactor," *Catal. Today*, **69**(1–4), 153 (2001a).
Heibel, A. K., T. W. J. Scheenen, J. J. Heiszwolf, H. Van As, F. Kapteijn, and J. A. Moulijn, "Gas and Liquid Phase Distribution and Their Effect on Reactor Performance in the Monolith Film Flow Reactor," *Chem. Eng. Sci.*, **56**(21–22), 5935 (2001b).
Heiszwolf, J. J., B. L. Engelvaart, G. M. van den Eijnden, T. M. Kreutzer, F. Kapteijn, and J. A. Moulijn, "Hydrodynamic Aspects of the Monolith Loop Reactor," *Chem. Eng. Sci.*, **56**(3), 805 (2001a).
Heiszwolf, J. J., M. T. Kreutzer, M. G. van den Eijnden, F. Kapteijn, and J. A. Moulijn, "Gas–Liquid Mass Transfer of Aqueous Taylor Flow in Monoliths," *Catal. Today*, **69**(1–4), 51 (2001b).
Highfill, W., and M. H. Al-Dahhan, "Liquid–Solid Mass Transfer Coefficient in High Pressure Trickle Bed Reactors," *Trans. IChemE*, **79**(A) (2001).
Iliuta, I., and F. Larachi, "Mechanistic Model for Structured-Packing Containing Columns Irrigated Pressure Drop, Liquid Holdup, and Packing Fractional Wetted Area," *Ind. Eng. Chem. Res.*, **40**, 5140 (2000).
Irandoust, S., and B. Andersson, "Mass Transfer and Liquid-Phase Reactions in a Segmented Two-Phase Flow Monolithic Catalyst Reactor," *Chem. Eng. Sci.*, **43**(8), 1983 (1988a).
Irandoust, S., and B. Andersson, "Monolithic Catalysts for Nonautomobile Applications," *Catal. Rev. Sci. Eng.*, **30**(3), 341 (1988b).
Irandoust, S., and B. Andersson, "Liquid Film in Taylor Flow through a Capillary," *Ind. Eng. Chem. Res.*, **28**(11), 1684 (1989a).
Irandoust, S., and B. Andersson, "Simulation of Flow and Mass Transfer in Taylor Flow through a Capillary," *Comput. Chem. Eng.*, **13**(4–5), 519 (1989b).
Irandoust, S., B. Andersson, E. Bengtsson, and M. Siverstroem, "Scaling Up of a Monolithic Catalyst Reactor with Two-Phase Flow," *Ind. Eng. Chem. Res.*, **28**(10), 1489 (1989c).
Irandoust, S., S. Ertle, and B. Andersson, "Gas–Liquid Mass Transfer in Taylor Flow through a Capillary," *Can. J. Chem. Eng.*, **70**(1), 115 (1992).
Irandoust, S., and O. Gahne, "Competitive Hydrodesulfurization and Hydrogenation in a Monolithic Reactor," *AIChE J.*, **36**(5), 746 (1990).
Kapteijn, F., T. A. Nijhuis, J. J. Heiszwolf, and J. A. Moulijn, "New Non-Traditional Multiphase Catalytic Reactors Based on Monolithic Structures," *Catal. Today*, **66**(2–4), 133 (2001).
Kawakami, K., K. Kawasaki, F. Shiraishi, and K. Kusunoki, "Performance of a Honeycomb Monolith Bioreactor in a Gas–Liquid–Solid Three-Phase System," *Ind. Eng. Chem. Res.*, **28**(4), 394 (1989).
Klinghoffer, A. A., R. L. Cerro, and M. A. Abraham, "Catalytic Wet Oxidation of Acetic Acid Using Platinum on Alumina Monolith Catalyst," *Catal. Today*, **40**(1), 59 (1998a).
Klinghoffer, A. A., R. L. Cerro, and M. A. Abraham, "Influence of Flow Properties on the Performance of the Monolith Froth Reactor for Catalytic Wet Oxidation of Acetic Acid," *Ind. Eng. Chem. Res.*, **37**(4), 1203 (1998b).
Kolb, W. B., and R. L. Cerro, "Coating the Inside of a Capillary of Square Cross Section," *Chem. Eng. Sci.*, **46**(9), 2181 (1991).
Kolb, W. B., and R. L. Cerro, "Film Flow in the Space between a Circular Bubble and a Square Tube," *J. Colloid Interface Sci.*, **159**(2), 302 (1993).
Kreutzer, M. T., P. Du, J. J. Heiszwolf, F. Kapteijn, and J. A. Moulijn, "Mass Transfer Characteristics of Three-Phase Monolith Reactors," *Chem. Eng. Sci.*, **56**(21–22), 6015 (2001).
Krishna, R., and S. T. Sie, "Strategies for Multiphase Reactor Selection," *Chem. Eng. Sci.*, **49**(24A), 4029 (1994).
Kumar, S. B., M. P. Dudukovic, J. Chaouki, F. Larachi, and M. P. Dudukovic, "Computer Assisted Gamma and X-ray Tomography: Applications to Multiphase Flow Systems," *Non-Invasive Monitoring of Multiphase Flows*, Elsevier, Amsterdam, pp. 47–103 (1997).
Lachman, I. M., and J. L. Williams, "Extruded Monolithic Catalyst Supports," *Catal. Today*, **14**(2), 317 (1992).
Lebens, P. J. M., J. J. Heiszwolf, F. Kapteijn, S. T. Sie, and J. A. Moulijn, "Gas–Liquid Mass Transfer in an Internally Finned Monolith Operated Countercurrently in the Film Flow Regime," *Chem. Eng. Sci.*, **54**(21), 5119 (1999a).
Lebens, P. J. M., F. Kapteijn, S. T. Sie, and J. A. Moulijn, "Potentials of Internally Finned Monoliths as a Packing for Multifunctional Reactors," *Chem. Eng. Sci.*, **54**(10), 1359 (1999b).
Lebens, P. J. M., M. M. Stork, F. Kapteijn, S. T. Sie, and J. A. Moulijn, "Hydrodynamics and Mass Transfer Issues in a Countercurrent Gas–Liquid Internally Finned Monolith Reactor," *Chem. Eng. Sci.*, **54**(13–14), 2381 (1999c).
Lebens, P. J. M., R. van der Meijden, R. K. Edvinsson, F. Kapteijn, S. T. Sie, and J. A. Moulijn, "Hydrodynamics of Gas–Liquid Countercurrent Flow in Internally Finned Monolithic Structures," *Chem. Eng. Sci.*, **52**(21–22), 3893 (1997).
Levenspiel, O., *The Chemical Reactor Omnibook*, OSU Book Stores, Inc., Corvallis, OR (1996).
Levenspiel, O., *Chemical Reaction Engineering*, Wiley, New York (1998).
Liu, W., "Ministructured Catalyst Bed for Gas–Liquid–Solid Multiphase Catalytic Reaction," *AIChE J.*, **48**(7), 1519 (2002).
Liu, W., W. P. Addiego, C. M. Sorensen, and T. Boger, "Monolith Reactor for the Dehydrogenation of Ethylbenzene to Styrene," *Ind. Eng. Chem. Res.*, **41**(13), 3131 (2002).
Marcandelli, C., A. S. Lamine, J. R. Bernard, and G. Wild, "Liquid Distribution in Trickle-Bed Reactor," *Oil Gas Sci Technol. Rev. IFP*, **55**(4), 407 (2000).
Mazzaroni, I., and G. Baldi, "Liquid-Phase Hydrogenation on a Monolith Catalyst," *Recent Trends in Chemical Reaction Engineering*, Vol. 2, B. D. Kulkarni, R.A. Mashelkar, and M. M. Sharma, eds., Wiley Eastern Ltd. New Delhi, p. 181 (1987).
Mewes, D., T. Loser, and M. Millies, "Modelling of Two-Phase Flow in Packings and Monoliths," *Chem. Eng. Sci.*, **54**(21), 4729 (1999).
Mishima, K., and T. Hibiki, "Some Characteristics of Air–Water Two-Phase Flow in Small Diameter Vertical Tubes," *Int. J. Multiphase Flow*, **22**(4), 703 (1996).
Mishima, K., and M. Ishii, "Flow Regime Transition Criteria for Upward Two-Phase Flow in Vertical Tubes," *Int. J. Heat Mass Transfer*, **27**(5), 723 (1984).
Mishra, V. S., V. V. Mahajani, and J. B. Joshi, "Wet Air Oxidation," *Ind. Eng. Chem. Res.*, **34**(1), 2 (1995).
Nemec, D., G. Bercić, and J. Levec, "Gravimetric Method for the Deter-

mination of Liquid Holdup in Pressurized Trickle-Bed Reactors," *Ind. Eng. Chem. Res.*, **40**(15), 3418 (2001).
Nijhuis, T. A., F. M. Dautzenberg, and J. A. Moulijn, "Modeling of Monolithic and Trickle-Bed Reactors for the Hydrogenation of Styrene," *Chem. Eng. Sci.*, **58**, 1113 (2003).
Nijhuis, T. A., M. T. Kreutzer, A. C. J. Romijn, F. Kapteijn, and J. A. Moulijn, "Monolithic Catalysts as Efficient Three-Phase Reactors," *Chem. Eng. Sci.*, **56**(3), 823 (2001a).
Nijhuis, T. A., M. T. Kreutzer, A. C. J. Romijn, F. Kapteijn, and J. A. Moulijn, "Monolithic Catalysts as More Efficient Three-Phase Reactors," *Catal. Today*, **66**(2–4), 157 (2001b).
Patrick, R. H., Jr., T. Klindera, L. L. Crynes, R. L. Cerro, and M. A. Abraham, "Residence Time Distribution in Three-Phase Monolith Reactor," *AIChE J.*, **41**(3), 649 (1995).
Patrick, T. A., and M. A. Abraham, "Evaluation of a Monolith-Supported Pt/Al_2O_3 Catalyst for Wet Oxidation of Carbohydrate-Containing Waste Streams," *Environ. Sci. Technol.*, **34**, 3480 (2000).
Pinna, D., E. Tronconi, and L. Tagliabue, "High Interaction Regime Lockhart–Martinelli Model for Pressure Drop in Trickle-Bed Reactors," *AIChE J.*, **47**(1), 19 (2001).
Ramachandran, P. A., and R. V. Chaudhari, *Three-Phase Catalytic Reactors*, Gordon & Breach, New York (1983).
Reinecke, N., and D. Mewes, "Flow Regimes of Two Phase Flow in Monolith Catalyst," Proc. of the 5th World Congress on Chemical Engineering, San Diego, CA (1996).
Reinecke, N., and D. Mewes, "Oscillatory Transient Two-Phase Flows in Single Channels with Reference to Monolithic Catalyst Supports," *Int. J. Multiphase Flow*, **25**(6–7), 1373 (1999).
Reinecke, N., G. Petritsch, D. Schmitz, and D. Mewes, "Tomographic Measurement Techniques—Visualization of Multiphase Flows," *Chem. Eng. Technol.*, **21**, 7 (1998).
Roy, S., A. K. Heibel, W. Liu, and T. Boger, "Design of Monolithic Catalysts for Multiphase Reactions," Oral Presentation, 17th SCRE (2002).
Satterfield, C. N., and F. Ozel, "Some Characteristics of Two-Phase Flow in Monolithic Catalyst Structures," *Ind. Eng. Chem. Fundam.*, **16**(1), 61 (1977).
Schluter, V., and W. D. Deckwer, "Gas–Liquid Mass Transfer in Stirred Vessels," *Chem. Eng. Sci.*, **47**, 2357 (1992).
Schöön, N. H., "Recent Progress in Liquid-Phase Hydrogenation: With Aspects from Microkinetics to Reactor Design," Proc. of the 6th Natl. Sympos. Chem. React. Eng., Warsaw, Poland (1989).
Schutt, B. D., B. Serrano, R. L. Cerro, and M. A. Abraham, "Production of Chemicals from Cellulose and Biomass-Derived Compounds through Catalytic Sub-Critical Water Oxidation in a Monolith Reactor," *Biomass & Bioenergy*, **22**(5), 365 (2002).
Smits, H. A., A. Stankiewicz, W. C. Glasz, T. H. A. Fogl, and J. A. Moulijn, "Selective Three-Phase Hydrogenation of Unsaturated Hydrocarbons in a Monolithic Reactor," *Chem. Eng. Sci.*, **51**(11), 3019 (1996).
Stankiewicz, A., "Process Intensification in In-Line Monolithic Reactor," *Chem. Eng. Sci.*, **56**(2), 359 (2001).
Stankiewicz, A. I., and J. A. Moulijn, "Process Intensification: Transforming Chemical Engineering," *Chem. Eng. Prog.*, **96**(1), 22 (2000).
Thulasidas, T. C., M. A. Abraham, and R. L. Cerro, "Bubble-Train Flow in Capillaries of Circular and Square Cross Section," *Chem. Eng. Sci.*, **50**(2), 183 (1995a).
Thulasidas, T. C., M. A. Abraham, and R. L. Cerro, "Dispersion during Bubble-Train Flow in Capillaries," *Chem. Eng. Sci.*, **54**(1), 61 (1999).
Thulasidas, T. C., R. L. Cerro, and M. A. Abraham, "The Monolith Froth Reactor: Residence Time Modeling and Analysis," *Chem. Eng. Res. Des.*, **73**(A3), 314 (1995b).
Triplett, K. A., S. M. Ghiaasiaan, S. I. Abdel-Khalik, A. LeMouel, and B. N. McCord, "Gas–Liquid Two-Phase Flow in Microchannels. Part II: Void Fraction and Pressure Drop," *Int. J. Multiphase Flow*, **25**(3), 395 (1999a).
Triplett, K. A., S. M. Ghiaasiaan, S. I. Abdel-Khalik, and D. L. Sadowski, "Gas–Liquid Two-Phase Flow in Microchannels. Part I: Two-Phase Flow Patterns," *Int. J. Multiphase Flow*, **25**(3), 377 (1999b).
Van't Riet, K., "Review of Measuring Methods and Results in Nonviscous Gas–Liquid Mass Transfer in Stirred Vessels," *Ind. Eng. Chem. Proc. Dev.*, **18**, 357 (1979).
Williams, J. L., "Monolith Structures, Materials, Properties and Uses," *Catal. Today*, **69**(1–4), 3 (2001).
Woehl, P., and R. L. Cerro, "Pressure Drop in Monolith Reactors," *Catal. Today*, **69**(1–4), 171 (2001).
Zhao, T. S., and Q. C. Bi, "Co-Current Air–Water Two-Phase Flow Patterns in Vertical Triangular Microchannels," *Int. J. Multiphase Flow*, **27**(5), 765 (2001).

Manuscript received July 14, 2003, and revision received Feb. 29, 2004.